



SHIRSHOV INSTITUTE OF OCEANOLOGY

CRUISE REPORT No. 45

RV *AKADEMIK IOFFE* CRUISE 15 - 26 September 2014

**North Atlantic Repeat Hydrography of sill sections
between Greenland - Iceland - Faroe Islands and Shetlands**

Principal Scientists **S Gladyshev**¹

2015

Shirshov Institute of Oceanology
36 Nakhimovskii prospect
Moscow 117997 RUSSIA
Tel: +7(495) 719 0255 Fax:
+7(499) 124 6342 Email:

sgradyshev@ocean.ru

¹Shirshov Institute of
Oceanology

DOCUMENT DATA SHEET

AUTHOR GLADYSHEV, S	PUBLICATION DATE 2015
TITLE RV <i>Akademik Ioffe</i> Cruise 45 , 15 - 26 September 2014.	
REFERENCE Shirshov Institute of Oceanology, Akademik Ioffe Cruise Report, No. 45, 67pp. tables & figs.	

ABSTRACT

RV *Akademik Ioffe* Cruise 45 was a contribution to the RUSSIA CLIVAR Community Research Programme. The sections over North Atlantic sills between Greenland - Iceland - Faroe Islands and Shetlands were designed to estimate variability of the meridional fluxes and water mass exchange between the North Atlantic and the Arctic Ocean. The Denmark Strait section was repeated three times during six days to study short-term variability of the water mass properties circulation and meridional transport.

KEYWORDS

CRUISE 45 2014, AKADEMIK IOFFE, CLIVAR, DENMARK STRAIT, NORTH ATLANTIC SILLS, INTEROCEAN EXCHANGE, CTD OBSERVATIONS, VMADCP, LADCP

ISSUING ORGANISATION

Shirshov Institute of Oceanology
36 Nakhimovskii prospect
Moscow 117997 RUSSIA

Director: Academician Robert Nigmatulin

Copies of this report are available from: **Department of Marine Operations**, Tel: +7(495)7190255 Fax: +7(499)124 6342

Email: sgladyshv@ocean.ru

Contents

Scientific Personnel

1. Cruise Narrative

1.1 Cruise Details

1.2 Cruise Summary

1.2.1 Cruise Track and Stations

1.2.2 Equipment

1.2.3 Sampling

1.2.4 Number of Stations Occupied

1.3 Scientific Objectives

1.4 Narrative

1.4.1 Introduction

1.4.2 Deep convection in the Irminger Sea

1.4.3 Reverse of the deep water freshening

1.4.4 Deep ocean salinity changes and NAO

1.4.5 Deep ocean salinity changes and climate change

1.4.6 Decadal variability of the DWBC at Cape Farewell

1.4.7 Mean state of the full depth circulation in 2000s

1.4.8 Cascading of dense shelf water in the Irminger Sea

1.5 Preliminary Results

1.6 Major Problems and Goals not achieved

2. Continuous Measurements (on station and underway)

2.1 Navigation

2.2 Meteorological Measurements

2.3 Thermosalinograph

2.4 Echosounding

2.5 Vessel Mounted Acoustic Doppler Current Profiler (OS 38 kHz)

3. On-Station Measurements

3.1 CTD

3.1.1 Equipment

3.1.2 Data processing and calibration

3.1.3 Final post-cruise CTD calibration

3.1.4 SBE 43 dissolved oxygen sensor calibration using Winkler Titration

3.2 Oxygen Bottle Samples

3.3 Lowered Acoustic Doppler Current Profiler (LADCP)

3.3.1 LADCP Processing for Current Profile

4. Cruise Logistics

5. Acknowledgements

Tables

Figures

Scientific Personnel

GLADYSHEV, S. PYATAKOV, V.	Principal Scientist Chief of CTD group	Shirshov Shirshov Atlantic Branch
GLADYSHEV, V. ZAPOTYL'KO, V. AGARKOV, A. NECHVOLODOV, L. KULESHOV, A.	CTD, LADCP, Sampling CTD, LADCP, Sampling CTD, LADCP, Sampling Sampling Winch	Shirshov Shirshov Shirshov Shirshov Shirshov Atlantic Branch
LUKASHIN, S.	Winch	Shirshov Atlantic Branch
DUKHOVA, L. KOLOKOLOVA, A. BULYCHEV, V.	Chief of Chemistry Group Oxygen Oxygen, Sampling	Shirshov Shirshov Shirshov Atlantic Branch
KABANOVA, E. GLADYSHEVA, S.	Nutrients Salinity	Shirshov Shirshov
KRINITSKII, M. GAVRIKOV, A.	Meteo Meteo	Shirshov Shirshov
SANTANA, M.	CO ₂	University of Las Palmas
ALVARADO, R.	CO ₂	University of Las Palmas
SUMPERIO, G.	CO ₂	University of Las Palmas

1. CRUISE NARRATIVE

1.1 Cruise Details

Expedition Designation: R/V *Akademik Ioffe* Cruise 45, RUSSIA CLIVAR

Principal Scientists: Dr Sergey V. Gladyshev (Shirshov).

Ship: RV *Akademik Ioffe*.

Ports of Call: Reykjavik (Iceland) to Rotterdam (Netherlands).

Cruise Dates: 15th September to 26th September 2014.

1.2 Cruise Summary

1.2.1 Cruise Track and Stations

The cruise track with station positions is shown in **Fig. 1**. Only small volume samples were taken, details are listed in **Table 1**.

1.2.2. Equipment

The principal instruments used during the cruise were a SBE 9P-743 CTD with dual temperature and conductivity sensors (SBE 3 SN 03P5677, SBE 4 SN 042827, SBE 3 SN 03P4401, SBE 4 SN 042925), oxygen sensor (SBE 43, SN 430699, SN 430727), turbidity sensor (SeaPoint Turbidity, SN 10218 STM), Benthos altimeter model PSA-900D, LADCP WHS-300 kHz down-looking (S/N 6393), LADCP WHS-300 kHz up-looking (S/N 14151). These were mounted together with a multisampler Carousel SBE 32 equipped with 22 5-litre Niskin bottles. Upon recovery each bottle was sampled in turn for dissolved oxygen, nutrients, salinity. All sampling was done on deck. Currents were measured using vessel mounted ADCP (VMADCP) TRDI OS38 kHz (S/N 1185) installed at the central point of the ship hull.

Navigation information was provided by a Trimble SPSx50/SPSx51 - Modular GPS receiver and every second was recorded on the PC. Additional measurements were made with an ELAC 12 kHz, Aanderaa meteorological package.

1.2.3 Sampling

Nominal depths sampled were: bottom, 1100, 1000, 900, 800, 700, 600, 500, 400, 300, 200, 150, 100, 50, 30, 20, 10 m. On deep casts fewer shallow and intermediate bottles were fired. The actual bottle depths are shown in **Fig. 2**.

1.2.4 Number of Stations Occupied

85 stations (87 casts) were occupied during the cruise that includes sections between Greenland and Iceland (2 repeats), Faroe and Iceland, Shetlands and Faroe (1 repeat) (**Fig. 1**).

1.3 Scientific Objectives

The cruise objectives were to:

1. To complete a CTD section from the Great Britain to Greenland.
2. To survey the North Atlantic sills with high-resolution CTD and LADCP/VMADCP data to determine the circulation and meridional fluxes.

1.4 Narrative

1.4.1 Introduction

The Meridional overturning circulation (MOC) in the North Atlantic is one of the main drivers of the widely known global oceanic “conveyor belt” – an important element of the Earth’s climate system [e.g., [van Aken, 2007](#)]. Warm upper-ocean waters transported northward by the North Atlantic Current release heat to the atmosphere, gain density due to cooling and eventually sink in the subpolar North Atlantic and adjacent Arctic seas thereby generating the return southward flow of colder waters at depths (**Fig. 3**) [[Dickson and Brown, 1994](#); [Koltermann et al., 1999](#)]. Temporal variability of the large-scale circulation and associated heat transport in the subpolar North Atlantic is one of the principal factors behind the high-latitude climate anomalies in the Northern Hemisphere.

Progress in understanding the causes of the ongoing climate change and forecasting climate variability in the Arctic and over European part of Russia for the next decades require reliable observation-based estimates of the variability of the North Atlantic circulation and the

Atlantic–Arctic heat and freshwater fluxes, as well as elucidation of the underlying mechanisms. In a number of recent studies, radical changes in the thermohaline regime and large-scale circulation in the Atlantic Ocean have been suggested to occur under global warming. For instance, the long-term freshening of the subpolar North Atlantic deep waters since the mid-1960s [Dickson et al., 2002] has been (cautiously) attributed to climate change-related factors [Curry et al., 2003; Hansen et al., 2004]. Hypothetically, under global warming, an increased evaporation in the tropics and increased precipitation at high latitudes, coupled with an intensified melting of Arctic ice, lead to the upper-ocean freshening in the regions of deep water formation and, hence, to the deep water freshening in the Atlantic Ocean. At the same time, milder winters along with the upper-ocean freshening lead to a decrease in the deep water production rates, which results in slowing of the Atlantic Meridional Overturning Circulation [e.g., Hansen et al., 2004; Bryden et al., 2005].

To better understand the past and present changes in the ocean-atmosphere dynamical system, as well as their causes and consequences, data on the full-depth oceanic variability are needed. An indispensable effective tool for assessing the large-scale circulation and thermohaline changes in the deep ocean and investigating mechanisms governing these changes are repeated full-depth transoceanic observations.

Since 1997, the P.P. Shirshov Institute of Oceanology has carried out the long-term monitoring of the North Atlantic circulation and water mass properties in the 59.5°N hydrographic section between Cape Farewell (Greenland) and Scotland (**Fig. 3**). Since 2002, the section has been repeated yearly on board the Russian research vessels, providing high precision data on temperature, salinity, oxygen and nutrients concentrations, and current velocities in the entire water column – “from shore to shore”, from the sea surface to the bottom. In 2011-2014, in addition to annual repeat measurements at 59.5°N, the P.P. Shirshov Institute of Oceanology started full-depth repeat observations of the oceanic exchange between the Atlantic and Arctic oceans through the straits between Greenland, Iceland, Faeroe and Shetland Islands (**Fig. 3**). The full-depth observations – of the same oceanic quantities as at 59.5°N – are performed in the straits from research vessels twice a year, in summer and fall. Based on the unique data set thus collected, a number of fundamental findings have already been achieved. Below, we briefly summarize the main subjects and results of our research.

The 59.5°N transatlantic section (**Fig. 3**) was designed for monitoring the large-scale circulation and thermohaline / chemical properties of oceanic waters at the northern periphery of the NA – the region where the warm upper-ocean waters are transformed by deep convection and mixing into the colder intermediate and deep waters – the Labrador Sea Water (LSW), Iceland Scotland Overflow Water (ISOW) and Denmark Strait Overflow Water (DSOW) (**Fig. 3**) – transported southward in the lower limb of the Atlantic MOC. Hydrographic data collected at 59.5°N along with those obtained within the framework of the kindred projects, primarily the French OVIDE (<http://www.ifremer.fr/lpo/ovide>), and historical data sets have been used for studying the dense water production [Falina et al., 2007; Falina et al., 2012], decadal temperature and salinity changes in the intermediate–deep water column [Sarafanov et al., 2007; Sarafanov et al., 2008; Sarafanov et al., 2010b], causes of these changes [Sarafanov, 2009; Sarafanov et al., 2010b], the mean state [Sarafanov et al., 2012] and long-term variability of the large-scale circulation in the region [Sarafanov et al., 2009; Sarafanov et al., 2010a; Våge et al., 2011].

1.4.2 Deep convection in the Irminger Sea

The oxygen data collected in 1997 in the northern North Atlantic in several sections ending nearby the southern tip of Greenland provided the observation-based support for the hypothesis [Pickart et al., 2003] that winter convection in the Irminger Sea may penetrate deep into the LSW layer (1000 – 2000 m) thus causing local renewal of this water mass. A separate lateral maximum of oxygen concentrations in the deep LSW layer was detected east of Cape Farewell (59.5°N, 36–40°W): the concentrations increased (by ~0.1 ml/l) from the Labrador Sea eastern edge toward the Irminger Sea (**Fig. 4**) rather than the reverse, as would be expected if LSW observed in the Irminger Sea interior in 1997 were solely of advective origin [Falina et al., 2007].

1.4.3. Reversal of the deep-water freshening

The LSW and Nordic Seas overflow-derived deep waters, ISOW and DSOW, freshened in the northern North Atlantic during the last three–four decades of the 20th century [Dickson et al., 2002]. Between the 1960s and 1990s, the water column in the region freshened on average by about 0.03 [Curry et al., 2003].

The long-term freshening reversed in the mid-1990s [Sarafanov et al., 2007; Sarafanov et al., 2008; Sarafanov et al., 2010b]. The salinification (and warming) of the intermediate and deep waters since the mid-1990s (Fig. 5) was much more intense than the preceding freshening. Over nearly a decade (1997–2006), temperature / salinity in the intermediate–deep water column ($\sigma_0 \geq 27.45$, depths > 500–1000 m) at 59.5°N increased by $\sim 0.3^\circ\text{C} / 0.03\text{--}0.04$ [Sarafanov et al., 2008].

In the Irminger Sea, the long-term freshening in the deep water column ($\sigma_0 > 27.80$, depths > ~ 2000 m) reversed in the early 2000s [Sarafanov et al., 2010b]. The observed freshening reversal was a lagged consequence of the persistent ISOW salinification that occurred upstream, in the Iceland Basin, after 1996 due to salinification of the northeast Atlantic waters entrained into the overflow. It was demonstrated [Sarafanov et al., 2010b] that the entrainment salinity increase was associated with the North Atlantic Oscillation (NAO)-induced weakening and contraction of the Subpolar Gyre and corresponding northwestward advance of subtropical waters that followed the NAO decline in the mid-1990s and continued through the mid-2000s. Remarkably, the deep water freshening reversal was not related to changes in the overflow water salinity.

1.4.4. Deep-ocean salinity changes and the NAO

Close relationship between the thermohaline properties of the northern North Atlantic intermediate and deep waters and the winter NAO index on a decadal time scale ($r^2 \approx 0.65$, 1950s–2000s, Fig. 6b and 6c) was revealed [Sarafanov, 2009] from the observation-based salinity time series for LSW in the Labrador Sea [Yashayaev, 2007] and ISOW in the Iceland basin [Boessenkool et al., 2007; Sarafanov et al., 2007]. Persistent NAO decline (amplification) leads to warming and salinification (cooling and freshening) in the intermediate–deep water column.

An explanation for the close link between the NAO and the coherent decadal changes in the intermediate and deep water properties in the region was proposed [Sarafanov, 2009]. The two factors dominate this link (Fig. 6d): (i) intensity of convection in the Labrador Sea controlling injection of relatively cold fresh waters into the intermediate layer and (ii) zonal extent of the Subpolar Gyre that regulates the relative contributions of cold fresh subpolar waters

and warm saline subtropical waters to the entrainment into the Norwegian Sea overflow south of the Iceland–Scotland Ridge and to the Atlantic inflow to the Nordic Seas. These factors act in phase leading to the observed coherent thermohaline changes in the intermediate–deep water column.

Due to weakening of the surface forcing associated with the NAO transition into neutral to low phase (1950s to mid-1960s, mid-1990s to mid-2000s), convection in the Labrador Sea weakens diminishing cold fresh water penetration into the intermediate layer. This results in warming and salinification at the intermediate depths in the Subpolar Gyre. Concurrently, the Subpolar Gyre contracts allowing northward advance of warm saline upper-ocean and intermediate subtropical waters in the northeastern North Atlantic. Northward progression of subtropical waters increases temperature and salinity at the upper intermediate levels and, correspondingly, increases temperature and salinity of the northeast Atlantic waters entrained into the Iceland–Scotland overflow along its pathway to the deep Iceland basin. As a result, temperature and salinity at the deep levels increase. The contrary changes – intensification of deep convection in the Labrador Sea and expansion of the Subpolar Gyre – caused by amplifying surface forcing (mid-1960s to mid-1990s) lead to cooling and freshening at the intermediate–deep levels. Additionally, under high-NAO conditions, deep convection may occur in the Irminger Sea potentially contributing to cooling and freshening at the intermediate (LSW) levels. The two regimes of convection and large-scale circulation corresponding to stronger (early 1990s) and weaker (mid-1960s, mid-2000s) NAO-related atmospheric forcing are schematically visualized in **Fig. 7**.

1.4.5 Deep-ocean salinity changes and climate change

There are increasing concerns that in the warmer climate, the MOC may substantially decline due to a decrease in the convective activity in the northern North Atlantic and Nordic Seas [e.g., [Meehl et al., 2007](#)]. The long-term freshening in the Nordic Seas and freshening of the northern North Atlantic deep waters in the 1960s–1990s have been considered as a likely indicator or precursor of the dramatic change in the MOC [e.g., [Hansen et al., 2004](#)]. The freshening has been attributed to a combination of factors potentially associated with the global warming: the increasing ice melt and net precipitation at high latitudes [e.g., [Curry et al., 2003](#)]. A probable causality between the climate change and the decreasing North Atlantic deep water

salinity has supported the concerns and unfavorable predictions, thus ‘warming up’ the reasonable scientific debate on climate change and overblown speculations in media.

Despite the long-term increase in freshwater input to the Arctic, freshening in the northern North Atlantic had reversed in the mid-1990s, as we demonstrated above. This reversal forces us to revise the hypotheses on the mechanisms behind the deep-water thermohaline anomalies. It seems doubtful that the persistent global temperature growth may lead to the opposite decadal trends (positive-then-negative-then-positive, **Fig. 6**) in the deep water salinity.

Our results [[Sarafanov et al., 2008](#); [Sarafanov, 2009](#); [Sarafanov et al., 2010b](#)] suggest that natural atmospheric variability over the North Atlantic plays the major role in the deep-water thermohaline variability on a decadal time scale. There are no reasons to associate the deep-water freshening in the 1960s–1990s with climate change, unless the 3-decade-long surface forcing amplification is evidently shown to be a consequence of the latter. Having said that, the net 1950s–2000s trends in the water mass salinities are negative implying that the global factors (e.g., probable intensification of hydrological cycle [[Curry et al., 2003](#)]) may act on longer time scales.

1.4.6 Decadal variability of the Deep Western Boundary Current at Cape Farewell

Recent decadal changes in the Deep Western Boundary Current (DWBC) transport southeast of Cape Farewell were assessed from hydrographic data (1991–2007, **Fig. 7a**), direct velocity measurements (2002–2006) and satellite altimetry (1992–2007). Following the approach used in earlier studies [e.g., [Bacon, 1998](#)], we first determined that the DWBC ($\sigma_0 > 27.80$) baroclinic transport (T_{BC}) referenced to 1000 m depth increased by ~ 2 Sv between the mid-1990s (1994–1997) and 2000s (2000–2007) (**Fig. 8b**) [[Sarafanov et al., 2009](#)]. In the next step, we quantified velocity changes at the reference level (1000 m) by combining estimates of the hydrography-derived velocity changes in the water column and the altimetry-derived velocity changes at the sea surface [see [Sarafanov et al., 2010a](#)]. The inferred increase in the southward velocity at 1000 m above the DWBC in 1994–2007 indicates that the increase in the DWBC absolute transport was larger but very close to the 2-Sv increase in the DWBC T_{BC} . This result along with the observed coherence of the DWBC absolute and baroclinic transport changes between individual observations [[Sarafanov et al., 2010a](#)] imply that the DWBC absolute

transport variability in the region is well represented by its baroclinic component on decadal and shorter time scales.

The historical record of the DWBC T_{BC} (1955–2007, **Fig. 8c**) updated after Bacon [1998] shows distinct decadal variability (± 2 – 2.5 Sv) with the transport minima in the 1950s and mid-1990s, maximum in the early 1980s and moderate-to-high transport in the 2000s. The DWBC T_{BC} decadal variability is consistent with the general pattern of the recent decadal hydrographic and circulation changes in the northern North Atlantic. The DWBC T_{BC} anomalies negatively correlate ($R = -0.80$, 1955–2007) with thickness anomalies of the Labrador Sea Water (LSW) at its origin implying a close link between the DWBC transport southeast of Cape Farewell and the LSW production in the Labrador Sea (**Fig. 8d**). During the recent three decades (late 1970s – late 2000s), the DWBC T_{BC} changes were also in-phase with changes in the strength and zonal extent of the Subpolar Gyre [see Sarafanov et al., 2010a]. In particular, the Gyre weakening at shallow levels in the mid-1990s – mid-2000s was accompanied by the DWBC strengthening in the Irminger Sea [Sarafanov et al., 2009; Sarafanov et al., 2010a; Våge et al., 2011]. The results imply that the decadal changes in the (i) LSW production, (ii) SPG strength and (iii) DWBC transport in the Irminger Sea are linked, representing a complex coherent oceanic response to the decadal variability of the surface forcing.

1.4.7 Mean state of the full-depth circulation in the 2000s

A mean state of the full-depth summer circulation in the Atlantic Ocean in the region in between Cape Farewell (Greenland), Scotland and the Greenland-Scotland Ridge (see **Fig. 3**) was assessed by combining 2002–2008 yearly hydrographic measurements at 59.5°N , mean dynamic topography, satellite altimetry data and available estimates of the Atlantic–Nordic Seas exchange [see Sarafanov et al., 2012]. The mean absolute transports by the upper-ocean, mid-depth and deep currents and the MOC ($\text{MOC}_{\sigma_0} = 16.5 \pm 2.2$ Sv, at $\sigma_0 = 27.55$) at 59.5°N were quantified in the density space. Inter-basin and diapycnal volume fluxes in between the 59.5°N section and the Greenland-Scotland Ridge were then estimated from a box model.

The estimated meridional and diapycnal volume fluxes contributing to the MOC are schematically visualized in **Fig. 9**. The dominant components of the meridional exchange across 59.5°N are the North Atlantic Current (NAC, 15.5 ± 0.8 Sv, $\sigma_0 < 27.55$) east of the Reykjanes Ridge, the northward Irminger Current (IC, 12.0 ± 3.0 Sv) and southward Western Boundary

Current (WBC, 32.1 ± 5.9 Sv) in the Irminger Sea and the deep water export from the northern Iceland Basin (3.7 ± 0.8 Sv, $\sigma_0 > 27.80$). About 60% (12.7 ± 1.4 Sv) of waters carried in the MOC σ upper limb ($\sigma_0 < 27.55$) by the NAC/IC across 59.5°N (21.1 ± 1.0 Sv) recirculates westwards south of the Greenland-Scotland Ridge and feeds the WBC. 80% (10.2 ± 1.7 Sv) of the recirculating NAC/IC-derived upper-ocean waters gains density of $\sigma_0 > 27.55$ and contributes to the MOC σ lower limb. Accordingly, the contribution of light-to-dense water conversion south of the Greenland-Scotland Ridge (~ 10 Sv) to the MOC σ lower limb at 59.5°N is one and a half times larger than the contribution of dense water production in the Nordic Seas (~ 6 Sv).

1.4.8 Cascading of dense shelf waters in the Irminger Sea

Based on the hydrographic data collected at 59.5°N , 64.3°N and $65\text{--}66^\circ\text{N}$ in the western Irminger Sea in the 1990s – 2000s, an observational evidence for the deep-reaching cascading of dense shelf waters south of the Denmark Strait was found [Falina et al., 2012]. The data collected in the northwestern Irminger Sea ($65\text{--}66^\circ\text{N}$) indicate that the East Greenland Current ~ 200 km south of the Denmark Strait occasionally carries shelf waters as dense as the overflow-derived deep waters transported by the DWBC ($\sigma_0 > 27.80$). Hydrographic traces of cascading of dense shelf waters down the East Greenland slope were found from repeat measurements at 64.3°N , where the densest fresh plumes were observed within the DWBC ($\sigma_0 > 27.80$) (Fig. 10). Using the data collected at 59.5°N , we showed that the fresh ‘signals’ originating from the shelf can be traced in the DWBC as far downstream as the latitude of Cape Farewell, where the anomalously fresh oxygenated plumes are repeatedly observed in the ISOW and DSOW density classes.

The results of our analysis along with the results from earlier studies [e.g., Rudels et al., 1999; Rudels et al., 2002] indicate that shelf water cascading in the northern Irminger Sea is an intermittent process occurring in all seasons of the year. This implies that, despite the apparent short duration of a particular cascading event, the cumulative contribution of such events to the thermohaline variability and southward export of the deep waters in the WBC can be considerable. Our tentative estimate based on data from two synoptic surveys at $\sim 59.5^\circ\text{N}$ suggests that the transient contribution of a cascading event in the northern Irminger Sea to the DWBC transport at Cape Farewell can be as large as $\sim 25\%$.

References

1. Bacon, S. (1998), Decadal variability in the outflow from the Nordic seas to the deep Atlantic Ocean, *Nature*, *394*, 871–874.
2. Dickson, R. R., and J. Brown (1994), The production of North Atlantic Deep Water: Sources, rates and pathways, *J. Geophys. Res.*, *99*, C6, 12319–12341.
3. Dickson, R., Yashayaev, I., Meincke, J., Turrell, B., Dye, S., and J. Holfort (2002), Rapid freshening of the deep North Atlantic Ocean over the past four decades, *Nature*, *416*, 832–837.
4. Boessenkool, K. P., Hall, I. R., Elderfield, H., and I. Yashayaev (2007), North Atlantic climate and deep-ocean flow speed changes during the last 230 years, *Geophys. Res. Lett.*, *34*, L13614, doi:10.1029/2007GL030285.
5. Curry, R., Dickson, R., and I. Yashayaev (2003), A change in the freshwater balance of the Atlantic Ocean over the past four decades, *Nature*, *426*, 826–829.
6. Falina, A., A. Sarafanov, and A. Sokov (2007), Variability and renewal of Labrador Sea Water in the Irminger Basin in 1991–2004, *J. Geophys. Res.*, *112*, C01006, doi: 10.1029/2005JC003348.
7. Falina A., A. Sarafanov, H. Mercier, P. Lherminier, A. Sokov, and N. Daniault (2012), On the cascading of dense shelf waters in the Irminger Sea, *J. Phys. Oceanogr.*, doi:http://dx.doi.org/10.1175/JPO-D-12-012.1 (in press)
8. Hansen, B., Osterhus S., Quadfasel D., and W. Turrell (2004), Already the day after tomorrow?, *Science*, *305*, 953–954.
9. Hurrell, J. W. (1995), Decadal trends in the North Atlantic Oscillation: regional temperatures and precipitation, *Science*, *269*, 676–679.
10. Koltermann, K. P., A. Sokov, V. Tereschenkov, S. Dobroliubov, K. Lorbacher, and A. Sy (1999), Decadal changes in the thermohaline circulation of the North Atlantic, *Deep Sea Res., Part II*, *46*, 109–138, doi:10.1016/S0967-0645(98)00115-5.
11. Lherminier, P., H. Mercier, T. Huck, C. Gourcuff, F. F. Perez, P. Morin, A. Sarafanov, and A. Falina (2010), The Atlantic Meridional Overturning Circulation and the subpolar gyre observed at the A25–Ovide section in June 2002 and 2004, *Deep-Sea Res., Part I*, *57*, 1374–1391, doi:10.1016/j.dsr.2010.07.009.

12. Meehl, G. A., (2007), Global climate projections. *Climate Change 2007: The Physical Science Basis*, S. Solomon et al., Eds., Cambridge University Press, 747–847.
13. Pickart, R. S., Spall, M., Ribergaard, M. H., Moore, G. W. K. and R. Milliff (2003), Deep convection in the Irminger Sea forced by the Greenland tip jet, *Nature*, *424*, 152–156.
14. Rudels B., Eriksson P., Grönvall H., Hietala R. and Launiainen J. (1999), Hydrographic Observations in Denmark Strait in Fall 1997, and their Implications for the Entrainment into the Overflow Plume, *Geophys. Res. Lett.*, *26*, 1325–1328.
15. Rudels, B., E. Fahrbach, J. Meincke, G. Budeus, and P. Eriksson (2002), The East Greenland Current and its contribution to the Denmark Strait overflow, *ICES J. Marine Science*, *59*, 1133–1154.
16. Sarafanov, A., A. Sokov, A. Demidov, and A. Falina (2007), Warming and salinification of intermediate and deep waters in the Irminger Sea and Iceland Basin in 1997–2006, *Geophys. Res. Lett.*, *34*, L23609, doi:10.1029/2007GL031074.
17. Sarafanov, A., A. Falina, A. Sokov, and A. Demidov (2008), Intense warming and salinification of intermediate waters of southern origin in the eastern subpolar North Atlantic in the 1990s to mid-2000s, *J. Geophys. Res.*, *113*, C12022, doi:10.1029/2008JC004975.
18. Sarafanov, A. (2009), On the effect of the North Atlantic Oscillation on temperature and salinity of the subpolar North Atlantic intermediate and deep waters, *ICES J. Marine Science*, *66* (7), 1448–1454, doi:10.1093/icesjms/fsp094.
19. Sarafanov, A., A. Falina, H. Mercier, P. Lherminier, and A. Sokov (2009), Recent changes in the Greenland–Scotland overflow-derived water transport inferred from hydrographic observations in the southern Irminger Sea, *Geophys. Res. Lett.*, *36*, L13606, doi:10.1029/2009GL038385.
20. Sarafanov A., A. Falina, P. Lherminier, H. Mercier, A. Sokov, and C. Gourcuff (2010a), Assessing decadal changes in the Deep Western Boundary Current absolute transport southeast of Cape Farewell (Greenland) from hydrography and altimetry, *J. Geophys. Res.*, *115*, C11003, doi:10.1029/2009JC005811.
21. Sarafanov A., H. Mercier, A. Falina, A. Sokov, and P. Lherminier (2010b), Cessation and partial reversal of deep water freshening in the northern North Atlantic: observation-

- based estimates and attribution, *Tellus*, 62A, 80–90, doi:10.1111/j.1600-0870.2009.00418.x.
22. Sarafanov A., A. Falina, H. Mercier, A. Sokov, P. Lherminier, C. Gourcuff, S. Gladyshev, F. Gaillard, and N. Daniault (2012), Mean full-depth summer circulation and transports at the northern periphery of the Atlantic Ocean in the 2000s, *J. Geophys. Res.*, 117, C01014, doi:10.1029/2011JC007572.
 23. Schmitz, W. J., Jr., and M. S. McCartney (1993), On the North Atlantic Circulation, *Rev. Geophys.*, 31, 29–49.
 24. Schott, F. A., and P. Brandt (2007), Circulation and deep water export of the subpolar North Atlantic during the 1990s, in *Ocean Circulation: Mechanisms and Impacts*, *Geophys. Monograph Series*, 173, Eds. A. Schmittner, J. Chiang, and S. Hemmings, 91–118, doi:10.1029/173GM08.
 25. Sutherland, D. A., and R. S. Pickart (2008), The East Greenland Coastal Current: structure, variability, and forcing, *Prog. Oceanogr.*, 78, 58–77, doi:10.1016/j.pocean.2007.09.006.
 26. Våge K., R. Pickart, A. Sarafanov, Ø. Knutsen, H. Mercier, P. Lherminier, H. van Aken, J. Meincke, D. Quadfasel, and S. Bacon (2011a), The Irminger Gyre: circulation, convection, and interannual variability, *Deep-Sea Res. Part I*, 58, 590–614, doi:10.1016/j.dsr.2011.03.001.
 27. van Aken, H. M. (2007), *The oceanic thermohaline circulation: An introduction*, New York, Springer, 326 p., ISBN 978-0-387-36637-1.
 28. Yashayaev, I. (2007), Hydrographic changes in the Labrador Sea, 1960–2005, *Prog. Oceanogr.*, 73, 242–276.

1.5 Preliminary Results

The upper-ocean, mid-depth and deep water circulation patterns, merging the results of the present analysis with those from the earlier studies [e.g., *Macrander et al.*, 2005; *Østerhus et al.*, 2005, 2008; *Schott and Brandt*, 2007; *Sutherland and Pickart*, 2008; *Lherminier et al.*, 2010; *Våge et al.*, 2011], are schematically visualized Figures 12–14. A schematic diagram of the meridional overturning circulation in the Atlantic Ocean north of 59.5°N is displayed in Fig. 9.

The results provide the following conceptual view of the gyre / overturning circulation at the northern periphery of the Atlantic Ocean in the 2000s.

The NAC and IC collectively carry 21.1 ± 1.0 Sv of warm upper-ocean waters across 59.5°N northwards within the MOC σ upper limb ($\sigma_0 < 27.55$). About 40% of this flow forms the Atlantic Inflow to the Nordic Seas, and 60% (12.7 ± 1.4 Sv) recirculates westwards in the subpolar gyre northern limb south of Iceland to feed the WBC in the Irminger Sea. Only 20% (2.4 ± 1.2 Sv) of the recirculating NAC/IC-derived waters exits the Irminger Sea in the WBC at shallow levels ($\sigma_0 < 27.55$), while 80% (10.2 ± 1.7 Sv, a half of the NAC/IC northward flow across 59.5°N) gains density of $\sigma_0 > 27.55$ and enters the MOC σ lower limb. The resulting net southward transport in the MOC σ lower limb at the latitude of Cape Farewell is 16.5 ± 2.2 Sv, of which ~60% (~10.2 Sv) is due to light-to-dense water transformation south of the GSR.

As no dense-to-light water re-conversion is expected to occur in the subpolar gyre, the NAC/IC-derived waters, once entering the MOC σ lower limb in the Irminger Sea, will eventually contribute to the MOCz lower limb (~11 Sv at 59.5°N) at the southern margin of the subpolar region. There, at ~48°N, the MOC σ and MOCz are of nearly the same magnitude, 16 ± 2 Sv, as estimated from data collected in the 1990s [see *Schott and Brandt*, 2007; *Lumpkin et al.*, 2008]. This is very close to our estimate of the mean MOC σ at 59.5°N. The comparison is tentative, though, because it does take into account the decadal variability of the MOC [Koltermann *et al.*, 1999; Willis, 2010]. With this caveat in mind, our results imply a minor contribution to the MOC σ by the net dense water formation in the subpolar gyre between ~48°N and 59.5°N. This inference concurs with the results by *Pickart and Spall* [2007] suggesting a

minor contribution to the Atlantic MOC by the net water mass transformation in the Labrador Sea.

To conclude, the results of the present study, verified with independent estimates where possible, provide the first observation-based quantitative view of a mean state of the gyre / overturning circulation at the northern periphery of the Atlantic Ocean. The most interesting features of the obtain circulation pattern are as follows:

- Nearly half of volume of the upper-ocean waters transported northward across 59.5°N in the eastern limb of the subpolar gyre (NAC and IC, $\sigma_0 < 27.55$) overturns in the density plane south of the GSR and feeds the lower limb of the Atlantic MOC σ .
- The contribution to the MOC σ lower limb at 59.5°N by overturning (light-to-dense transformation) of the NAC / IC-derived upper-ocean waters south of the GSR is one and a half times as large as the contribution of the Nordic Seas overflows.
- The net southward flow in MOC σ lower limb at 59.5°N is associated primarily with the deep water ($\sigma_0 > 27.80$) export. Nearly half of the net southward flow of deep waters across 59.5°N is due to entrainment of the Atlantic waters in the Irminger Sea.
- The DWBC at 59.5°N is fed primarily by the Denmark Strait Overflow and by the diapycnal flux / entrainment from the mid-depth layer, while the contribution to the DWBC transport from the ISOW flow is minor. A major part of the ISOW transported into the Irminger Sea from the Charlie-Gibbs Fracture Zone recirculates southward in the eastern Irminger Sea and exits the basin via an interior pathway rather than along the western boundary. The results can be used for validation of numerical models. From this perspective, multi-year mean transports have an obvious advantage over individual section-based synoptic estimates, which bear the impress of vigorous variability occurring on a variety of spatial and temporal scales. The methodological outcome is that the combined use of repeat hydrography, the MDT by *Rio and Hernandez* [2004] and satellite altimetry data can provide a useful estimate of the mean full-depth circulation across a transatlantic section without imposing *a priori* constraints.

1.6 Major Problems and Goals Not Achieved

Sta # 3242 was repeated because of the CTD cable flooding during up-cast #1. During Sta #3308 (cast #1) one of the oil hoses was broken when the CTD was near the bottom. Sta #3308 was repeated after the hose replacement. Bottle #12 upper lanyard was broken during attachment to the trigger hook before Sra #3242. Broken lanyard was replaced within 15 minutes. GPS data did not transmit to the Echosounder PC between Sta ##3247-3250. The problem was fixed after proxy Data PC rebooting. Bottle #4 did not close during Sta #3257. Bottle #3 leaked during Sta #3279. Bottle #4 leaked during Sta #3309..

2. CONTINUOUS MEASUREMENTS (on station and underway)

2.1 Navigation

Navigation data from Trimble SPSx50/SPSx51 GPS was recorded every 1 second and was stored on the PC in binary format.

2.2 Meteorological Measurements

The standard mean meteorological measurements were stored in the separate files on the same PC with navigation data. Recording were running immediately after departure from Reykjavik (Iceland) on 15th September, and worked reliably until completion of the cruise in Rotterdam (Netherlands) on 26th September.

2.3 Thermosalinograph

SBE 21 S/N 3254 data were collected along the section line starting on September 16th.

2.4 Echosounding

The bathymetric equipment aboard during RV Akademik Ioffe Cruise 45 consists of an ELAC 12 kHz hydrographic echosounder. Data were collected for most of the cruise. The Hull mounted transducer is located 5.8 metres below the sea surface and this value was entered to estimate the depth.

Depth was indicated on the echosounder display and stored on the PC together with the navigation.

Two files with extension NAV and MET with maximum size 256032 b were created. File name corresponded to GMT time when the file was opened for records.

2.5 Vessel Mounted Acoustic Doppler Current Profiler (VMADCP) OS 38 kHz

The Ocean Surveyor 38 kHz is designed for vessel-mount current profile measurement in the upper ocean water from depths greater than 40-50 meters. The system consists of a transducer and electronics chassis connected to PC. Data are transmitted in binary format through the I/O cable. GPS data in NMEA format are transmitted separately to another PC COM – port. The VMADCP can operate in two regimes (Narrow Bandwidth and Broad Bandwidth Profiling). Its main specifications are shown below.

To collect OS 38 kHz data we used *VmDas* software (version 1.46). The NMEA messages *VmDas* reads are standard GGA, HDG, HDT, VTG messages.

	Bin size	Maximum range	Accuracy (cm/s) ²
NarrowBand (long-range mode)	16 m	800 - 1000 m	30
	24 m	900 - 1200 m	23
BroadBand (high-precision mode)	16 m	520 - 730 m	12
	24 m	730 – 780 m	9

We used a following configuration to collect the data.

NP00001 – Narrow Bandwidth profiling

NN060 – number of bins 60

NS1600 – cell size 24 m

NF1600 – blanking size 16 m

BP00 – no bottom track (BP),

VmDas saves data in a few files with extension ENX, ENS, ENR (raw data with and without navigation), NR – NMEA messages, STA and LTA averaged data. Misalignment angle was introduced in configuration file and was used by VmDas for data correction.

Data processing performed STA files with 40-profile averaging. Taking into account that single ping takes about 3 seconds, one 40-profile ensemble lasts near 120 seconds in Narrow Bandwidth regime.

Data processing consists of data conversion in NetCDF format with extension NC and further cleaning, filtering, tide removing (using barotropic tidal model TPXO 7.2) and averaging. The standard space averaging was 3 km. IFREMER software was used to process OS 38 kHz data.

3. ON-STATION MEASUREMENTS

3.1 CTD

3.1.1 Equipment

The deep profiler system used during the cruise included the following components: SBE 32 painted aluminum 24 bottle multisampler frame, SBE 9P-0743 CTD, spare SBE 9P-0767, CTD Up and Down looking RD Instruments WHS – 300 kHz Acoustic Doppler Current Profiler (LADCP), Separate Battery pack pressure case ext. 6000 m connected to LADCPs with star cable, 24 x 5 litre Test Oceanic Niskin bottles, Benthos altimeter PSA-900D.

Lab equipment for data acquisition and archiving of CTD/LADCP data consisted of the following items mounted on the deck.

Pentium IV – Intel 2.2 GHz, PC Intel Core 2 Duo 2.4GHz Personal Computers. APC Back-UPS 550VA/330W, SBE 11p Deck Unit.

Cruise Preparation

Equipment and sensors were assembled when the ship moved to the first station from Reykjavik (15-16th September). Water bottles were checked for integrity of seals, taps, stoppers and lanyards before being fitted and roped to the multisampler frame.

Deployment

The CTD performed well during the cruise with little evident instrument drift and good accuracy.

The CTD was deployed with a lowering rate of 60 metres/min (30-40 metres/min in the upper 200 metres or deeper if the conditions are rough). It is recovered at a rate of 60 metres/min.

The LADCPs fitted within the frame with a separate battery pressure case performed well. These units contain a compass and tilt sensors which could possibly provide useful information on the attitude and rotation of the whole profiler package throughout deployments.

Bottle firing using the deck unit and pylon was very reliable during the cruise.

Operationally this has been a successful cruise with virtually no time being lost due to mechanical or equipment failure.

3.1.2 Data processing and calibration

CTD data were logged at 24 scans per second and passed from the CTD deck unit to the PC.

The CTD data was recorded onto disk by the PC using SEABIRD SEASOFT-Win 32: Seasave 7, Software Release 7.21d. A screen display of temperature, oxygen, salinity and density profiles vs pressure are used to decide the depths at which bottles are to be tripped on the up cast. The bottles are tripped using the enable and fire buttons on the PC screen. During post-processing, the SEASAVE software stores 35 scans at each bottle trip within a separate file. At the end of the station, all the data and header files associated with the station are transferred immediately via ethernet to the second PC. The SBE data processing software is used to create 1 dbar processed data files.

The data processing takes the following steps:

DATCNV Converts the raw data to physical parameters.

WILDEDIT For every block of 100 scans, flags all scans whose pressure, temperature, conductivity and oxygen values differ from the mean by more than 2 standard deviations. Recomputes mean from unflagged data then marks as bad all scans exceeding 20 standard deviations from these new values.

FILTER Low pass filter pressure channel with time constant used for pressure 0.150 seconds.

ALIGNCTD Aligns the oxygen values relative to the pressure values accounting for the time delays in the system. Time offsets of 4.000 secs for oxygen are used.

CELLTM A recursive filter used to remove the thermal mass effects from the conductivity data. Thermal anomaly amplitude and time constants of 0.0300 and 7.0000 were used.

LOOPEDIT Marks as bad, all cycles on the down trace for which the vertical velocity of the CTD unit is less than 0.25 metres/sec.

WINDOW FILTER cosine filter temperature and conductivity, window size 23 scans.

DERIVE Computes salinity, potential temperature, sigma-t, sigma theta and oxygen values.

BINAVG Averages the down cast into 1 dbar pressure bins.

SPLIT Splits the data into DOWN and UP cast.

Calibration data

The CTD calibrations used during this cruise were supplied by Sea Bird Electronics and are as follows:

Pre-cruise calibration:

CALIBRATION DATE: 24-Jun-2014 (all stations)

Conductivity Sensor S/N 042827

$h = 1.36977079e+000$
 $i = 5.01531580e-004$
 $j = 2.74090064e-005$
 $CP_{cor} = -9.5700e-008$
 $CT_{cor} = 3.2500e-006$

Post-cruise calibration:

CALIBRATION DATE: 04-Jun 2015 (all stations)

Conductivity Sensor S/N 042827

$g = -1.00469063e+001$
 $h = 1.37383902e+000$
 $i = -6.26359501e-004$
 $j = 1.11707771e-004$
 $CP_{cor} = -9.5700e-008$ (nominal)
 $CT_{cor} = 3.2500e-006$ (nominal)
 Average drift between *pre* and *post-cruise* calibrations: -0.00010 PSU/month (at 3.0 S/m)

Pre-cruise calibration:

CALIBRATION DATE: 19-Jun-14 (all stations)

Temperature Sensor S/N 035677

Temperature ITS-90 = $1/\{g + h[\ln(f_0/f)] + i[\ln^2(f_0/f)] + j[\ln^3(f_0/f)]\} - 273.15$ (°C)
 Following the recommendation of JPOTS: T68 is assumed to be $1.00024 * T90$ (-2 to 35°C)
 f is the frequency
 $g = 4.29395484e-003$
 $h = 6.23609246e-004$
 $i = 1.89843091e-005$
 $j = 1.41258435e-006$
 $f_0 = 1000.0$

Post-cruise calibration:

CALIBRATION DATE: 19-Jun-14 (sta. 3040-3132)

Temperature Sensor S/N 035677

Temperature ITS-90 = $1/\{g + h[\ln(f_0/f)] + i[\ln^2(f_0/f)] + j[\ln^3(f_0/f)]\} - 273.15$ (°C)
 Following the recommendation of JPOTS: T68 is assumed to be $1.00024 * T90$ (-2 to 35°C)
 f is the frequency
 $g = 4.29395484e-003$
 $h = 6.23609246e-004$
 $i = 1.89843091e-005$
 $j = 1.41258435e-006$
 $f_0 = 1000.0$

Average drift between *pre* and *post-cruise* calibrations: +0.00000 degrees Celsius/year

Pressure Sensor S/N 89105 (sta. 3040-3132) no drift

CALIBRATION DATE: 27-June-11

$C1 = -4.905371e+004$
 $C2 = -1.210594e+000$
 $C3 = 1.428350e-002$
 $D1 = 3.901600e-002$
 $D2 = 0.000000e+000$
 $T1 = 3.001017e+001$

$T2 = -5.758384 \times 10^{-4}$
 $T3 = 4.210120 \times 10^{-6}$
 $T4 = 2.265400 \times 10^{-9}$
 $T5 = 0.000000 \times 10^{+000}$
 $AD590M = 1.28912 \times 10^{-2}$
 $AD590B = -8.43097 \times 10^{+000}$
 Slope = 0.99995
 Offset = 1.4284 (dbars)

Oxygen Sensor 430699

CALIBRATION DATE: 18-Dec-2014 (sta. 3040-3132)

$$\text{Oxygen(ml/l)} = \{Soc * (V + Voffset)\} * Oxsat(T,S) * e^{(Tcorr*T)} * e^{(Pcor*P)}$$

Where:

V = SBE 43 output voltage signal (volts)

T = CTD temperature (°C)

S = CTD salinity (psu)

P = CTD pressure (dbars)

$Oxsat(T,S)$ = oxygen saturation (ml/l)

Soc , $Voffset$, $tcor$, and $pcor$ are calibration coefficients

Let:

$$\phi = Oxsat(T,S) * e^{(Tcorr*T)} * e^{(Pcor*P)}$$

$$\text{Oxygen(ml/l)} = Soc * (V + Voffset) * \phi$$

$$\text{Oxygen(ml/l)} / \phi = Soc * (V + Voffset) = M * V + B$$

Where:

$$Soc = M$$

$$Voffset = B / M$$

In our case for sill sections

$$Soc = 4.1214 \times 10^{-001}$$

$$\text{Tau} = 0.0$$

$$Boc = 0.0000$$

$$Voffset = -0.3524$$

$$tcor = 0.001700$$

$$pcor = 1.35 \times 10^{-004}$$

3.1.3 Final Post-Cruise CTD Calibrations

Temperature Calibration Temperature Sensors S/N 035677 (SBE 9P-0743),

We applied zero correction for the primary sensors S/N 035677 and we used *pre-cruise calibration coefficients* for all stations of the cruise).

Pressure Calibration Pressure Sensor S/N 89105

Final CTD pressure correction: Since no drift for pressure sensor was defined by SeaBird Electronics pressure was corrected for atmospheric pressure only. With offset in *.con* or *.xmlcon* file set to -0.0026 db, pressure measured by CTD should equal barometric pressure

- Calculate offset (db) = barometer reading – CTD reading
- Conversion of psia to decibars: decibars = (psia - 14.7) * 0.6894759
- Enter calculated offset in *.con* or *.xmlcon* file
- Example:
 - CTD reads -2.5 dbars
 - Barometer reads 14.65 psia.

Converting to decibars, barometer reads $(14.65 - 14.7) * 0.6894759 = -0.034$ dbars

– offset (db) = barometer reading – CTD reading = $-0.034 - (-2.5) = 2.466$

Salinity Calibration Conductivity Sensor S/N 042827

We used *pre-cruise calibration coefficients* for all stations of the cruise with zero sensor slope correction. We defined this using *post-cruise calibration* and by taking 256 salinity samples from depth deeper than 250 m between 16 and 24 September 2014. These samples were measured with Autosal 8400 B laboratory salinometer (S/N 67465) during 5 runs between 18 and 25 September. The results of these measurements are shown in **Fig. 11a**. The first run was done after annual Autosal Factory Service including cell cleaning. This cleaning caused difficulties in cell filling at the beginning because of bad wetting. Thus Run #1 was not perfect. The drift of both sensors between Runs #2 and #5 was around 0.0005 PSU during the cruise and the mean difference between Autosal and CTD was within the accuracy of measurements in the ship laboratory (less than 0.002 PSU).

Description of Equipment and Technique

Salinity samples are analyzed on Guildline Autosal model 8400 B salinometer. Samples are drawn in 150 ml dark glass medicine bottles. All bottles were equipped with plastic liners and caps. The salinometer cell is filled and rinsed three times with sample water before readings are recorded. Minimum three salinometer readings were recorded for every sample and standardization. If the values are fluctuating, more readings are taken.

Sampling Procedure and Data Processing Technique

Salinity samples are drawn into 150 ml medicine bottles after three rinses. The bottles are filled up to the shoulders and then capped with caps with plastic liners. Files for each separate run are prepared. These files consist of various metadata (date, cruise, lab temperature, geographic location, operator, etc.) and sample specific data such as the bath temperature, sample ID number, and average conductivity ratio. A PC based program computes the salinity using average conductivity ratio of the runs and the standard IAPSO formula. Any changes in the salinometer readings between successive standardizations are assumed to have occurred as a linear drift of the instrument. Thus, the program applies a correction to the ratios, which varies linearly with the samples analyzed. The salinity data is then placed in the water sample database.

Laboratory and Sample Temperatures

Full cases of samples are taken from the winch room to the salinometer lab where they are left for a period of at least 24 hours to equilibrate to laboratory temperature before being analyzed.

The bath in the salinometer was kept at 21°C.

Standards Used

The salinometer was standardized using IAPSO standard water, Batch P152, dated May, 2013. Standardization with a new bottle was carried out at the beginning and end of the run as well as after 50 bottle samples.

3.1.4 SBE 43 Dissolved Oxygen Sensor Calibration using Winkler Titrations

We use a method for statistically estimating calibration coefficients for calculating dissolved oxygen in milliliters per liter from SBE 43 output voltage. The technique requires dissolved oxygen concentration in ml/l (determined from Winkler titration of water samples) and SBE 43 oxygen voltage outputs at the times the water samples were collected. Sea-Bird's data processing software, SBE Data Processing, is used to produce a data table suitable for the analysis.

Background

The equation used in Sea-Bird's software for calculating dissolved oxygen in ml/l from SBE 43 output voltage is a form of that given in Owens-Millard (1985):

$$Oxygen(ml/l) = \{Soc * (V + Voffset + tau * \partial V/\partial t) + Boc * e^{(-0.03*T)}\} * Oxsat(T,S) * e^{(Tcorr*T)} * e^{(Pcor*P)} \quad eqn 1$$

Where:

V = SBE 43 output voltage signal (volts)

$\partial V/\partial t$ = time derivative of SBE 43 output signal (volts/second)

T = CTD temperature (°C)

S = CTD salinity (psu)

P = CTD pressure (dbars)

$Oxsat(T,S)$ = oxygen saturation (ml/l)

Soc , Boc , $Voffset$, tau , $tcor$, and $pcor$ are calibration coefficients

Characterization of the SBE 43 in the laboratory and ocean suggest that the most accurate results are obtained by setting Boc and tau to zero. Equation 1 then reduces to:

$$Oxygen(ml/l) = \{Soc * (V + Voffset)\} * Oxsat(T,S) * e^{(Tcorr*T)} * e^{(Pcor*P)} \quad eqn 2$$

The SBE 43 is expected to provide an output voltage that is linear with respect to oxygen concentration. Normal calibration drift manifests itself as a loss of sensitivity and is evident as a change of slope and offset in the linear relationship between oxygen concentration and voltage output. The coefficients $tcor$ and $pcor$ correct for small secondary responses to temperature and pressure. Because these coefficients change very slowly over time, the values given on the SBE 43 calibration certificate are used in this analysis.

Setting Boc and tau to zero, we will rearrange equation 2 into a linear form and perform a linear regression to obtain a new Soc and $Voffset$.

Let:

$$\phi = Oxsat(T,S) * e^{(Tcorr*T)} * e^{(Pcor*P)}$$

The oxygen equation then reduces to:

$$Oxygen(ml/l) = Soc * (V + Voffset) * \phi$$

This may be expressed in a linear form as shown in equation 3 below. A linear regression is calculated using Winkler oxygen concentration divided by ϕ as the dependent variable and SBE 43 output voltage as the independent variable.

$$Oxygen(ml/l) / \phi = Soc * (V + Voffset) = M * V + B \quad eqn 3$$

Where:

$$Soc = M$$

$$Voffset = B / M$$

Winkler oxygen divided by ϕ versus SBE 43 output voltage for this cruise is shown in

Fig. 12 and includes a linear regression line calculated from the data.

The *Soc* value is 4.1214e-001.

The *Voffset* value is -0.3524 for the sill sections

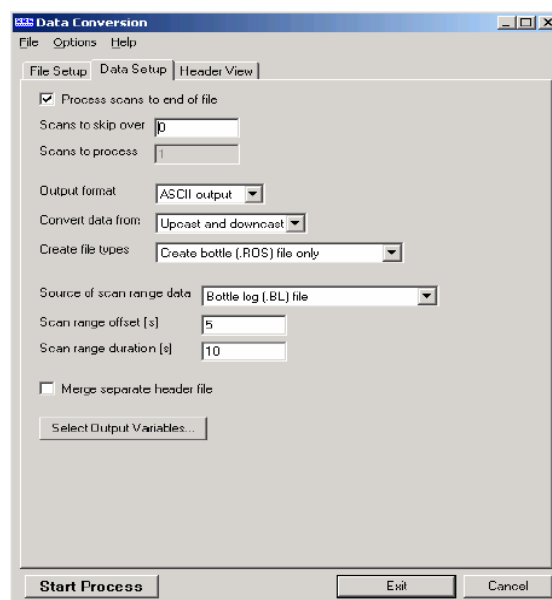
979 oxygen samples were used to build this linear fits.

Procedure

As a first step, extract pressure, temperature, salinity, oxygen saturation, and SBE 43 voltage from the parts of your CTD data collected when the water sampler closures occurred.

We run SBE Data Processing, and select Data Conversion in the Run menu. Select the appropriate configuration (.con) and data (.dat) files on the *File Setup* tab. In the *Data Setup* tab we set *Convert data from* to *Upcast and downcast* and *Create file types* to *Create bottle (.ROS) file only*.

To extract CTD data concurrent to the water sampler closures, Data Conversion must know when the closures occurred. Select an appropriate *Source of scan range data*, depending on your instrument type and how the sampler was commanded to close bottles:



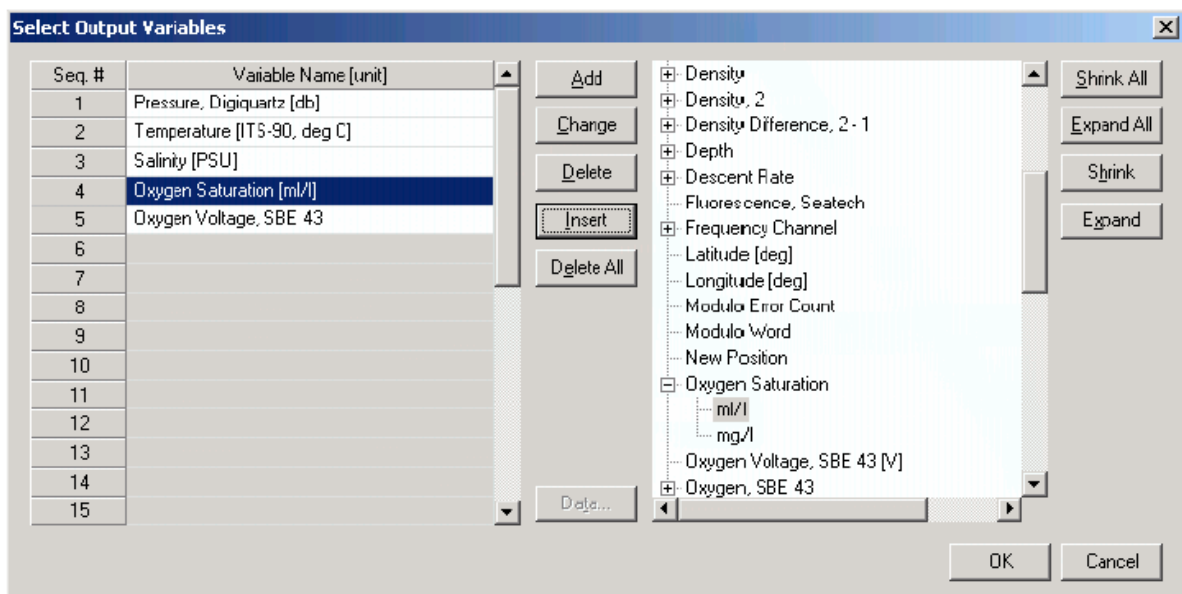
- SBE 9plus with SBE 11plus - The data stream is marked with a *bottle confirm* bit each time a closure occurred.

- Using SEASAVE to operate the water sampler - A *.bl* file, with scan ranges corresponding to closures, is created during the cast.

Like all sensors, the SBE 43 has a finite response time to a change in dissolved oxygen concentration. This response time is usually on the order of 6 seconds. For this reason, good sampling procedure dictates that the instrument package should be stopped in the water column long enough for the SBE 43 and all other sensors to completely equilibrate before closing the water sampler. An equilibration time of 5 to 6 response times, or 30 to 36 seconds, is adequate. We used to wait 30 seconds.

Data Conversion is extracting data 5 seconds before each water sampler closure and will extract 10 seconds of data. Note that 10 seconds is longer than the SBE 43 response time. Because we are extracting data for 5 seconds after the water sampler closure, the instrument package must remain stopped for at least this long.

To estimate *Soc* and *Voffset*, we need pressure, temperature, salinity, oxygen saturation (ml/l), and SBE 43 Oxygen Voltage to go with each Winkler titration data value. We use *Select Output Variables* and add each of the required parameters; the dialog box is shown below.



After selecting all the variables, click *OK* to return to the Data Conversion Data Setup tab. Then click *Start Process* to create the *.ros* file.

In our case, the *.ros* file contains 10 seconds of data centered on the moment the bottle closure occurred for every bottle closure. To make a useful table, we select Rosette Summary from SBE Data Processing's Run menu. Rosette Summary calculates averages and standard deviations for the variables selected in Data Conversion. Select the appropriate *.con* and *.ros* files

on the *File Setup* tab. To average the data in the *Data Setup* tab we click the *Select Averaged Variables* button; after selecting all the variables, click *OK* to return to the Rosette Summary Data Setup tab. Then click *Start Process* to create a data table file with the *.btl* extension.

Further, we run a program READBTLDATA to create a file with average pressure, temperature, salinity, oxygen saturation, and SBE 43 output voltage for each water sampler closure depth, by importing the *.btl* file and the Winkler titration dissolved oxygen values from our titration log, matching water sampler closures to number of station, bottle number and pressures. The program also calculates ϕ , using *tcor* and *pcor* from the SBE 43 calibration sheet.

Then, calculate *Winkler O₂/ ϕ* .

Using the table we perform a linear regression, with:

- *Winkler O₂/ ϕ* (shown as Winkler/phi in the table) as the *Y* data
- SBE 43 output voltages as the *X* data

Reference

Owens, W. B., and R. C. Millard Jr., 1985: A new algorithm for CTD oxygen calibration. *J. Physical Oceanography*, 15, 621-631.

(NOTE: calibration expressed as ml/l)

3.2 Oxygen Bottle Samples

Oxygen samples were drawn first from every bottle. Duplicate samples were taken on each cast, usually from the first two bottles. Samples were drawn into clear, wide necked calibrated glass bottles and fixed on deck with reagents dispensed using Aquastep bottle top dispensers. A test station used to check on the oxygen bottle calibrations and as an opportunity to train a number of people to take the samples. The samples were shaken on deck and again in the laboratory 1/2 hour after collection, when the bottles were checked for the tightness of the stoppers and presence of bubbles. The samples were then stored under water until analysis.

Bottle temperatures were taken, following sampling for oxygen, using a hand held electronic thermometer probe. The temperatures were used to calculate any temperature-dependent changes in the sample bottle volumes.

Samples were analyzed in the constant temperature laboratory, starting three hours after sample collection, following the Winkler whole bottle titration with an amperometric method of endpoint detection, as described by Culberson (1991). The equipment used was supplied by Metrohm and included

the Titrino unit and control pad, exchange unit with 10 ml burette to dispense the thiosulphate in increments of 2 μl , with an electrode for amperometric end point detection.

The difference for the duplicate pairs sampled on each station was in a range 0.00-0.02 ml/l (Table 2).

The thiosulphate normality was checked on each run and recalculated every time the reservoir was topped up against potassium iodate. The exact weight of this standard, the calibrated 5 ml exchange unit driven by a Metrohm Dosimat and the 1L glass volumetric flask used to dispense and prepare the standard.

The introduction of oxygen with the reagents and impurities in the manganese chloride were corrected for by blank measurements made on each run, as described in the WOCE Manual of Operations and Methods (Culberson, 1991).

In order to control the accuracy of the oxygen measurements at almost each cast were taken parallel sample from one bottle.

Reproducibility of measurements

1060 samples were taken during the cruise; including 70 duplicates. Statistics on the duplicates are given in Table 2. These include both duplicates taken from the same bottle (replicates) and those taken from different bottles fired at the same depth. This data gave a standard deviation of 0.007 ml/l.

References:

Culberson, C.H. 1991. 15 pp in the WOCE Operations Manual (WHP Operations and Methods) WHPO 91/1, Woods Hole.

Modern methods of hydrochemical research of the ocean, 1992. IO RAS, Moscow (in Russian).

(L. Dukhova, A. Kolokolova)

3.3 Lowered Acoustic Doppler Current Profiler (LADCP)

The TRDI WHS 300 kHz ADCPs consists of a pressure case rated to 6000 metres with 4 transducers at one end in a convex arrangement and the beams diverging at 20 degrees from the vertical. At the opposite end to the transducers is a connector that enables downloading of data and connects it to other pressure cases containing another ADCP and the power supply pack. This arrangement allowed the ADCPs and the battery pack to be mounted vertically as up and down-looking on the CTD frame. Connection amongst all units was established using star cable with three male and two female terminations. Two male cable ends were always attached to the frame, this enabled comms leads to be readily connected pre and post deployment.

Communications: The 20-m communication leads (which also allow external power to be supplied to the ADCP) were sufficiently long to route it through to the port side of the deck lab where it was connected to a dedicated PC and external power supply. The latter was set at 48+ volts and was left on whilst the ADCP was on deck. 5 minutes prior to deployment the external power supply was shut off, the instrument checked and the configuration file sent to the ADCP as described in the manual instructions. The free end of the fly leads was greased and the end cap refitted, this was then taped to the frame for security.

Post deployment: When the CTD/LADCP was brought inboard, the fly-lead connectors were dried and the comms leads were connected to them. This stopped undue bending of the cables and kept them clear of the water bottles, aiding sampling. External power was applied again and the cast data downloaded as per the manual with a baud rate of 57600. The processing is accomplished using software developed by Visbeck after transferring the data to the PC.

Battery power was supplied to the ADCP in the form of 42 volts from 28 x 1.5 volt alkaline cells. Four of these packs were available for the cruise, as the ADCP will function at a minimum of 32 volts this was deemed an adequate stock for the duration.

Data quality: The data quality from the ADCP was good throughout. Due to the bad weather instrument titles sometimes exceeded 12° and this data was rejected during processing.

The LADCPs seem to function well and generates useful information on currents. The battery supply has its limitations though and thought should be given to alternatives to the present set-up.

3.3.1 LADCP Processing for Current Profiles

A brief account of the LADCP current data processing, file nomenclature and directory structure is provided in the following lines. Little emphasis is put into a detailed description of the main programming tools used, since these are part of a standard software package developed by Gerd Krahnemann (version 10.13).

Outline of LADCP current calculation method

The Broad Band LADCP used during AI42 cruise was designed to measure the instantaneous relative velocities of scatterers in the water column by taking advantage of the Doppler frequency shift, phase changes and correlation between coded pulses transmitted and received by the LADCP's four transducers. Conversion of this raw data stream to a profile of absolute currents involved an elaborate calculation method.

Firstly, Doppler shifts needed to be scaled to velocity units by taking into account the depth-dependent sound velocity (estimated from CTD T and S measurements). Directions could be inferred from trigonometric calculations based on the geometry of the transducer set, the orientation of the package

(measured with a flux gate compass) and the local magnetic declination. The depth of the instrument was calculated from the integration of the measured vertical velocity and later adjusted to match the depth given by the CTD's pressure sensor.

The velocities corresponding to each single ensemble (or, in effect, to each transducer ping) were gridded in bins of depth set 10 meters. Statistical rejection of spiky measurements within each of these bins followed.

In order to reject the unwanted motion of the instrument (but also the barotropic component of the current), shear profiles were calculated for each ensemble. A complicated editing scheme preceded this shear calculation. A final shear profile (baroclinic current) was derived by real- depth gridding of the shear profiles calculated for individual ensembles. It was hoped that any relative velocities introduced by the high-frequency motion of the CTD package would be smoothed out by this repeated averaging.

The barotropic component of the flow was finally calculated from bottom-tracking measurements (bottom-track mode) or, in most occasions, in an integral sense from differential GPS positions of the ship (water-track mode).

The definitive velocity profile was hence obtained as the sum of the baroclinic and barotropic components.

During AI42 cruise, no specific error calculation was performed. Profiles of shear standard deviation were included in the cast log sheet folder. Internal wave signals were obvious throughout the cruise.

Relevant PC files

The raw data were downloaded from the LADCP into a devoted PC after each cast and stored as a binary file called vNNNNm_01.000 for Master and vNNNNs_01.000 for Slave the c:\ladcp\AI45\dNNN directory, where NNNN stands for the CTD cast number, e.g. raw data from cast 3303 were stored in the files d:\AI45\data\ladcp\v3303m_01.000 and v3303s_01..000.

The configuration files (named Mconf.txt and Sconf.txt) containing the operating instructions (setting of track mode, bin depth, etc.) given to the LADCP previously to deployment was stored in the same directory.

Text files of the form NNNNm.log and NNNNs.log are the log of the 'bbtalk' session (testing the state and functioning of the instrument) previous to deployment. The details of the sessions for every single cast in the cruise are to be found in the cast log sheets.

A whole variety of files were created and manipulated during the different processing stages, and no mention will be made of the majority of them for reasons of clarity. The processing procedure may be summarised in two steps:

1- create CTD pressure, temperature and salinity data file as well as navigation collected every second in order to obtain the best possible estimates of depth and sound velocity. This is done using 'SBE Data Processing software and ConvLADCP Fortran program.

2- use the Gerd Krahnmann's standard matlab package (v. 10.13) with P. Lherminier's improvements (IFREMER) to process LADCP and CTD data

References

M. Visbeck 2002: Deep Velocity Profiling using Lowered Acoustic Doppler Current Profiler: Bottom Track and Inverse Solutions J. Atmos. Oceanic Technol. 10, 764-773.

4. CRUISE LOGISTICS

Mobilization

Mobilization for the cruise took place on the way from Reykjavik (Iceland) to the first station of the cruise. It took twelve hours. The scientific team arrived at the ship on September 15th.

ACKNOWLEDGEMENTS

The principal scientists would like to thank the Master, officers, crew and scientists of the RV Akademik Ioffe for making this such an enjoyable, as well as successful cruise.

TABLES

Table 1. CTD casts

Table 2. Performance of chemical analysis along the sill sections in 45 cruise R/V *Akademik Ioffe*

FIGURES

Fig. 1. Station location and ship track (in red). The shelf area with depth less than 200 m is shaded.

Fig. 2. Vertical distribution of samples along the sill sections.

Fig. 3. Schematic diagram of the large-scale circulation in the northern North Atlantic compiled from [Schmitz and McCartney, 1993; Schott and Brandt, 2007; Sutherland and Pickart, 2008; Lherminier et al., 2010]. Abbreviations for the main topographic features, currents and water masses are explained in the legend. The nominal locations of the 59.5°N hydrographic section (1997 – present) and sections across the straits between Greenland, Iceland, Faeroe and Shetland Islands (2011 – present) are shown with the solid green lines.

Fig. 4. Oxygen concentrations (ml/l) in the water column (lower panel) as observed in March–October 1997 in four hydrographic sections (upper panel) ending nearby the southern tip of Greenland. A separate oxygen maximum in the LSW layer (1000–2000 m) in the Irminger Sea at 59.5°N strongly implies local convective renewal of LSW before 1997. Adapted from [Falina et al., 2007].

Fig. 5. Warming and salinification in the northern North Atlantic between the mid-1990s and mid-2000s, as observed at 59.5°N. The figure shows the 2006–1997 temperature (°C, left) and salinity (right) differences on isobaric surfaces in the Irminger Sea and Iceland Basin. Adapted from [Sarafanov et al., 2007].

Fig. 6. Coherence of the decadal salinity changes (1950s – 2000s) of the intermediate (LSW) and deep (ISOW) waters in the northern North Atlantic and their link to the North Atlantic Oscillation (NAO) index. **(a)** Schematic representation of the LSW and ISOW pathways and locations of the Icelandic Low (L) and Azores High (H) centers constituting the NAO dipole pattern. The red dotted line indicates the 59.5°N transatlantic section. **(b)** Salinity time series for LSW in the Labrador Sea [Yashayaev, 2007] and ISOW in the Iceland basin [Boessenkool et al., 2007; Sarafanov et al., 2007] overlaid by the third order polynomial fits. **(c)** Time series of the winter NAO index, after [Hurrell, 1995], overlaid by 7-year running mean and third order polynomial fit. **(d)** Mechanism of the NAO effect on the decadal changes in temperature (T) and salinity (S) of the northern North Atlantic intermediate and deep waters. Positive / negative links shown with the dark / light grey arrows mean that changes in ‘causative’ and ‘consequential’ characteristics have the same / opposite sign(s). The overall effect of the NAO on T and S of the in the water column is negative: persistent NAO decline leads to warming and salinification of the water masses and vice versa, as shown in (b) and (c). Adapted from [Sarafanov, 2009].

Fig. 7. Schematic representation of the upper-ocean circulation and convection intensity in the northern North Atlantic under high (left) and low (right) NAO conditions. Blue (magenta) solid arrows indicate the upper-ocean flows with higher fraction of colder fresher subpolar (warmer saltier subtropical) waters. The main pathways of the Nordic overflow-derived deep waters are shown with the dotted curves. “C” and “E” symbols are used to denote, respectively, the deep convection sites and the domain, where the Atlantic waters are entrained into ISOW. Larger (smaller) circles indicate stronger (weaker) convection. SPG and STG – the subpolar and subtropical gyres, respectively. Adapted from [Sarafanov, 2009].

Fig. 8. The Deep Western Boundary Current (DWBC) transport variability and its link to the convection intensity in the Labrador Sea. **(a)** Locations of the hydrographic sections (1991–2007) and schematic of the deep water circulation in the Irminger Sea. **(b)** The DWBC transport anomalies at Cape Farewell in 1991–2007, $1 \text{ Sv} = 10^6 \text{ m}^3 \text{ s}^{-1}$. The 1994–1997 and 2000–2007 mean anomalies and the 1994–2007 linear trend are shown. **(c)** Anomalies of the DWBC transport at Cape Farewell and the Labrador Sea Water (LSW) thickness in the Labrador Sea in the 1950s–2000s. **(d)** Correlation coefficient (R^2) for the two times series shown in **(c)** at the 0–5-year lag, the LSW thickness leads. The correlation maximum is achieved at the 1–3-year lag. The DWBC transport anomalies in the southern Irminger Sea are foregone by the convection intensity anomalies in the Labrador Sea. Adapted from [Sarafanov et al., 2009].

Fig. 9. Schematic diagram of the Meridional Overturning Circulation (MOC) at the northern periphery of the Atlantic Ocean, northeast of Cape Farewell. The dotted lines refer to the σ_0 isopycnals 27.55 and 27.80. The arrows denote the integral meridional and diapycnal volume fluxes. Where the signs are specified, the positive (negative) transports are northward (southward). The NAC and EGIC transports in the upper layer ($\sigma_0 < 27.55$) at 59.5°N are the throughputs accounting for the recirculations. EGIC – the East Greenland / Irminger Current – refers to the upper part of the Western Boundary Current. Other abbreviations are explained in the legend to **Fig. 3**. Adapted from [Sarafanov et al., 2012].

Fig. 10. Salinity observed in the northwestern Irminger Sea at 64.3°N in February 1998. The σ_0 isopycnals 27.55, 27.70, 27.80 and 27.88 are plotted as the thick black lines; the station locations are marked with the ticks on the top axis. The plot shows fresh dense waters descending (cascading) down the continental slope of Greenland down to the LSW layer ($27.70 < \sigma_0 < 27.80$) and the layer of the Nordic Seas overflow-derived deep waters ($\sigma_0 > 27.80$). Adapted from [Falina et al., 2012].

Fig. 11. Autosal 8400B CTD salinity offset for the primary (in black) and secondary (in red) conductivity sensors (a) SBE 9P 0743 based on 256 salinity samples (5 runs) during 45 cruise of R/V *Akademik Ioffe*. Vertical bars show standard deviation of each run. Thick lines denote linear fits.

Fig. 12. Regression line for Winkler oxygen divided by ϕ versus SBE 43 output voltage for the sill sections.

Fig. 13. The vertical distribution of potential temperature (a, b) and salinity (c, d) between Greenland and Iceland 16-18 September 2014 and 18-19 September 2014. Density is shown in black.

Fig. 14. The vertical distribution of dissolved oxygen between Greenland and Iceland 16-18 September 2014 and 18-19 September 2014. Density is shown in black.

Fig. 15. The vertical distribution of potential temperature (a) and salinity (b) between Iceland and Faroe Islands 21-22 September 2014. Density is shown in black.

Fig. 16. The vertical distribution of dissolved oxygen between Iceland and Faroe Islands 21-22 September 2014. Density is shown in black.

Fig. 17. The vertical distribution of potential temperature (a) and salinity (b) between Shetlands and Faroe Islands 23-24 September 2014. Density is shown in black.

Fig. 18. The vertical distribution of dissolved oxygen between Shetlands and Faroe Islands 23-24 September 2014. Density is shown in black.

STATION	CAST	TYPE	DATE	TIME	CODE	LATITUDE	LONGITUDE	NAV	DEPTH	BOTTOM	BOTTLES	COMMENTS
3231	1	ROS	091614	0834	BE	65 34.8 N	024 54.9 W	GPS	67	4	6	CTD,LADCP,O2,SiO3,PO4,CO2
3231	1	ROS	091614	0840	BO	65 34.8 N	024 54.8 W	GPS	67	4	6	CTD,LADCP,O2,SiO3,PO4,CO2
3231	1	ROS	091614	0849	EN	65 34.8 N	024 54.8 W	GPS	67	4	6	CTD,LADCP,O2,SiO3,PO4,CO2
3232	1	ROS	091614	1006	BE	65 39.9 N	025 15.7 W	GPS	86	2	7	CTD,LADCP,O2,SiO3,PO4,CO2
3232	1	ROS	091614	1015	BO	65 39.9 N	025 15.9 W	GPS	86	2	7	CTD,LADCP,O2,SiO3,PO4,CO2
3232	1	ROS	091614	1024	EN	65 39.9 N	025 15.9 W	GPS	86	2	7	CTD,LADCP,O2,SiO3,PO4,CO2
3233	1	ROS	091614	1141	BE	65 44.9 N	025 38.3 W	GPS	267	3	12	CTD,LADCP,O2,SiO3,PO4,CO2
3233	1	ROS	091614	1153	BO	65 45.0 N	025 38.6 W	GPS	267	3	12	CTD,LADCP,O2,SiO3,PO4,CO2
3233	1	ROS	091614	1209	EN	65 45.0 N	025 38.5 W	GPS	267	3	12	CTD,LADCP,O2,SiO3,PO4,CO2
3234	1	ROS	091614	1323	BE	65 49.9 N	025 59.8 W	GPS	222	4	11	CTD,LADCP,O2,SiO3,PO4,CO2
3234	1	ROS	091614	1331	BO	65 49.9 N	025 59.9 W	GPS	222	4	11	CTD,LADCP,O2,SiO3,PO4,CO2
3234	1	ROS	091614	1345	EN	65 49.9 N	025 59.8 W	GPS	222	4	11	CTD,LADCP,O2,SiO3,PO4,CO2
3235	1	ROS	091614	1532	BE	65 55.9 N	026 28.7 W	GPS	286	4	12	CTD,LADCP,O2,SiO3,PO4,CO2
3235	1	ROS	091614	1543	BO	65 56.0 N	026 28.9 W	GPS	286	4	12	CTD,LADCP,O2,SiO3,PO4,CO2
3235	1	ROS	091614	1601	EN	65 56.0 N	026 28.8 W	GPS	286	4	12	CTD,LADCP,O2,SiO3,PO4,CO2
3236	1	ROS	091614	1719	BE	66 00.9 N	026 47.8 W	GPS	442	3	14	CTD,LADCP,O2,SiO3,PO4,CO2
3236	1	ROS	091614	1732	BO	66 00.9 N	026 47.8 W	GPS	442	3	14	CTD,LADCP,O2,SiO3,PO4,CO2
3236	1	ROS	091614	1750	EN	66 00.9 N	026 47.6 W	GPS	442	3	14	CTD,LADCP,O2,SiO3,PO4,CO2
3237	1	ROS	091614	1848	BE	66 04.7 N	027 01.8 W	GPS	652	4	15	CTD,LADCP,O2,SiO3,PO4,CO2
3237	1	ROS	091614	1911	BO	66 05.0 N	027 02.9 W	GPS	652	4	15	CTD,LADCP,O2,SiO3,PO4,CO2
3237	1	ROS	091614	1941	EN	66 04.7 N	027 03.2 W	GPS	652	4	15	CTD,LADCP,O2,SiO3,PO4,CO2
3238	1	ROS	091614	2032	BE	66 08.9 N	027 14.7 W	GPS	517	5	15	CTD,LADCP,O2,SiO3,PO4,CO2
3238	1	ROS	091614	2051	BO	66 08.9 N	027 15.2 W	GPS	517	5	15	CTD,LADCP,O2,SiO3,PO4,CO2
3238	1	ROS	091614	2121	EN	66 08.4 N	027 15.9 W	GPS	517	5	15	CTD,LADCP,O2,SiO3,PO4,CO2
3239	1	ROS	091614	2210	BE	66 11.8 N	027 29.2 W	GPS	483	2	15	CTD,LADCP,O2,SiO3,PO4,CO2
3239	1	ROS	091614	2231	BO	66 11.8 N	027 30.2 W	GPS	483	2	15	CTD,LADCP,O2,SiO3,PO4,CO2
3239	1	ROS	091614	2253	EN	66 11.8 N	027 30.2 W	GPS	483	2	15	CTD,LADCP,O2,SiO3,PO4,CO2
3240	1	ROS	091614	2339	BE	66 14.7 N	027 44.2 W	GPS	468	3	16	CTD,LADCP,O2,SiO3,PO4,CO2
3240	1	ROS	091714	0000	BO	66 14.9 N	027 45.1 W	GPS	468	3	16	CTD,LADCP,O2,SiO3,PO4,CO2
3240	1	ROS	091714	0024	EN	66 14.9 N	027 45.1 W	GPS	468	3	16	CTD,LADCP,O2,SiO3,PO4,CO2
3241	1	ROS	091714	0133	BE	66 19.7 N	028 07.3 W	GPS	340	4	11	CTD,LADCP,O2,SiO3,PO4,CO2
3241	1	ROS	091714	0151	BO	66 19.9 N	028 08.5 W	GPS	340	4	11	CTD,LADCP,O2,SiO3,PO4,CO2

3241	1	ROS	091714	0208	EN	66 19.9 N	028 08.6 W	GPS	340	4	11	CTD,LADCP,O2,SiO3,PO4,CO2
3242	1	ROS	091714	0316	BE	66 24.8 N	028 30.4 W	GPS	297	4	4	CTD,LADCP,O2,SiO3,PO4,CO2
3242	1	ROS	091714	0332	BO	66 25.0 N	028 31.3 W	GPS	297	4	4	CTD,LADCP,O2,SiO3,PO4,CO2
3242	1	ROS	091714	0339	EN	66 25.0 N	028 31.3 W	GPS	297	4	4	CTD,LADCP,O2,SiO3,PO4,CO2
3242	1	ROS	091714	0357	BE	66 25.0 N	028 31.3 W	GPS	297	158	6	CTD,LADCP,O2,SiO3,PO4,CO2
3242	1	ROS	091714	0357	BO	66 25.0 N	028 31.3 W	GPS	297	158	6	CTD,LADCP,O2,SiO3,PO4,CO2
3242	1	ROS	091714	0401	EN	66 25.0 N	028 31.3 W	GPS	297	158	6	CTD,LADCP,O2,SiO3,PO4,CO2
3242	2	ROS	091714	0615	BE	66 25.1 N	028 31.4 W	GPS	297	5	13	CTD,LADCP,O2,SiO3,PO4,CO2
3242	2	ROS	091714	0625	BO	66 25.0 N	028 31.5 W	GPS	297	5	13	CTD,LADCP,O2,SiO3,PO4,CO2
3242	2	ROS	091714	0643	EN	66 25.1 N	028 31.5 W	GPS	297	5	13	CTD,LADCP,O2,SiO3,PO4,CO2
3243	1	ROS	091714	0754	BE	66 30.0 N	028 54.3 W	GPS	323	4	12	CTD,LADCP,O2,SiO3,PO4,CO2
3243	1	ROS	091714	0804	BO	66 29.9 N	028 54.4 W	GPS	323	4	12	CTD,LADCP,O2,SiO3,PO4,CO2
3243	1	ROS	091714	0819	EN	66 29.9 N	028 54.4 W	GPS	323	4	12	CTD,LADCP,O2,SiO3,PO4,CO2
3244	1	ROS	091714	0926	BE	66 34.9 N	029 15.9 W	GPS	302	3	13	CTD,LADCP,O2,SiO3,PO4,CO2
3244	1	ROS	091714	0940	BO	66 34.9 N	029 16.2 W	GPS	302	3	13	CTD,LADCP,O2,SiO3,PO4,CO2
3244	1	ROS	091714	0959	EN	66 34.9 N	029 16.2 W	GPS	302	3	13	CTD,LADCP,O2,SiO3,PO4,CO2
3245	1	ROS	091714	1104	BE	66 39.8 N	029 38.6 W	GPS	297	2	11	CTD,LADCP,O2,SiO3,PO4,CO2
3245	1	ROS	091714	1119	BO	66 39.8 N	029 39.0 W	GPS	297	2	11	CTD,LADCP,O2,SiO3,PO4,CO2
3245	1	ROS	091714	1132	EN	66 39.9 N	029 39.1 W	GPS	297	2	11	CTD,LADCP,O2,SiO3,PO4,CO2
3246	1	ROS	091714	1240	BE	66 45.0 N	030 02.6 W	GPS	327	4	12	CTD,LADCP,O2,SiO3,PO4,CO2
3246	1	ROS	091714	1254	BO	66 45.0 N	030 03.2 W	GPS	327	4	12	CTD,LADCP,O2,SiO3,PO4,CO2
3246	1	ROS	091714	1313	EN	66 45.1 N	030 03.3 W	GPS	327	4	12	CTD,LADCP,O2,SiO3,PO4,CO2
3247	1	ROS	091714	1421	BE	66 49.9 N	030 26.7 W	GPS	414	6	14	CTD,LADCP,O2,SiO3,PO4,CO2
3247	1	ROS	091714	1435	BO	66 50.0 N	030 27.1 W	GPS	414	6	14	CTD,LADCP,O2,SiO3,PO4,CO2
3247	1	ROS	091714	1452	EN	66 50.0 N	030 27.2 W	GPS	414	6	14	CTD,LADCP,O2,SiO3,PO4,CO2
3248	1	ROS	091714	1601	BE	66 55.0 N	030 49.6 W	GPS	576	3	15	CTD,LADCP,O2,SiO3,PO4,CO2
3248	1	ROS	091714	1617	BO	66 55.0 N	030 49.7 W	GPS	576	3	15	CTD,LADCP,O2,SiO3,PO4,CO2
3248	1	ROS	091714	1642	EN	66 55.0 N	030 49.7 W	GPS	576	3	15	CTD,LADCP,O2,SiO3,PO4,CO2
3249	1	ROS	091714	1747	BE	66 59.7 N	031 11.8 W	GPS	355	3	12	CTD,LADCP,O2,SiO3,PO4,CO2
3249	1	ROS	091714	1803	BO	67 00.0 N	031 12.7 W	GPS	355	3	12	CTD,LADCP,O2,SiO3,PO4,CO2
3249	1	ROS	091714	1820	EN	67 00.0 N	031 12.7 W	GPS	355	3	12	CTD,LADCP,O2,SiO3,PO4,CO2
3250	1	ROS	091714	1928	BE	67 04.7 N	031 35.1 W	GPS	295	5	12	CTD,LADCP,O2,SiO3,PO4,CO2
3250	1	ROS	091714	1943	BO	67 04.8 N	031 35.7 W	GPS	295	5	12	CTD,LADCP,O2,SiO3,PO4,CO2

3250	1	ROS	091714	2001	EN	67 04.8 N	031 35.7 W	GPS	295	5	12	CTD,LADCP,O2,SiO3,PO4,CO2
3251	1	ROS	091714	2107	BE	67 09.6 N	031 57.9 W	GPS	299	2	12	CTD,LADCP,O2,SiO3,PO4,CO2
3251	1	ROS	091714	2125	BO	67 09.8 N	031 59.2 W	GPS	299	2	12	CTD,LADCP,O2,SiO3,PO4,CO2
3251	1	ROS	091714	2142	EN	67 09.9 N	031 59.7 W	GPS	299	2	12	CTD,LADCP,O2,SiO3,PO4,CO2
3252	1	ROS	091714	2245	BE	67 14.9 N	032 21.1 W	GPS	365	2	12	CTD,LADCP,O2,SiO3,PO4,CO2
3252	1	ROS	091714	2306	BO	67 15.0 N	032 22.3 W	GPS	365	2	12	CTD,LADCP,O2,SiO3,PO4,CO2
3252	1	ROS	091714	2325	EN	67 14.9 N	032 22.6 W	GPS	365	2	12	CTD,LADCP,O2,SiO3,PO4,CO2
3253	1	ROS	091814	0109	BE	67 22.3 N	032 36.3 W	GPS	491	10	14	CTD,LADCP,O2,SiO3,PO4,CO2
3253	1	ROS	091814	0137	BO	67 22.3 N	032 34.6 W	GPS	491	10	14	CTD,LADCP,O2,SiO3,PO4,CO2
3253	1	ROS	091814	0159	EN	67 22.1 N	032 34.6 W	GPS	491	10	14	CTD,LADCP,O2,SiO3,PO4,CO2
3254	1	ROS	091814	0317	BE	67 30.5 N	032 47.4 W	GPS	313	3	12	CTD,LADCP,O2,SiO3,PO4,CO2
3254	1	ROS	091814	0331	BO	67 30.5 N	032 47.4 W	GPS	313	3	12	CTD,LADCP,O2,SiO3,PO4,CO2
3254	1	ROS	091814	0347	EN	67 30.5 N	032 47.4 W	GPS	313	3	12	CTD,LADCP,O2,SiO3,PO4,CO2
3255	1	ROS	091814	0451	BE	67 22.5 N	032 35.9 W	GPS	484	4	16	CTD,LADCP,O2,SiO3,PO4,CO2
3255	1	ROS	091814	0509	BO	67 22.3 N	032 34.6 W	GPS	484	4	16	CTD,LADCP,O2,SiO3,PO4,CO2
3255	1	ROS	091814	0533	EN	67 22.1 N	032 34.4 W	GPS	484	4	16	CTD,LADCP,O2,SiO3,PO4,CO2
3256	1	ROS	091814	0631	BE	67 15.0 N	032 22.4 W	GPS	368	4	11	CTD,LADCP,O2,SiO3,PO4,CO2
3256	1	ROS	091814	0647	BO	67 15.0 N	032 22.3 W	GPS	368	4	11	CTD,LADCP,O2,SiO3,PO4,CO2
3256	1	ROS	091814	0702	EN	67 15.0 N	032 22.4 W	GPS	368	4	11	CTD,LADCP,O2,SiO3,PO4,CO2
3257	1	ROS	091814	0813	BE	67 09.9 N	031 59.1 W	GPS	300	1	14	CTD,LADCP,O2,SiO3,PO4,CO2
3257	1	ROS	091814	0829	BO	67 09.8 N	031 59.2 W	GPS	300	1	14	CTD,LADCP,O2,SiO3,PO4,CO2
3257	1	ROS	091814	0847	EN	67 09.9 N	031 59.7 W	GPS	300	1	14	CTD,LADCP,O2,SiO3,PO4,CO2
3258	1	ROS	091814	0958	BE	67 04.9 N	031 36.0 W	GPS	296	5	10	CTD,LADCP,O2,SiO3,PO4,CO2
3258	1	ROS	091814	1013	BO	67 04.8 N	031 35.9 W	GPS	296	5	10	CTD,LADCP,O2,SiO3,PO4,CO2
3258	1	ROS	091814	1026	EN	67 04.8 N	031 36.2 W	GPS	296	5	10	CTD,LADCP,O2,SiO3,PO4,CO2
3259	1	ROS	091814	1139	BE	67 00.0 N	031 12.8 W	GPS	353	3	13	CTD,LADCP,O2,SiO3,PO4,CO2
3259	1	ROS	091814	1151	BO	66 59.9 N	031 12.9 W	GPS	353	3	13	CTD,LADCP,O2,SiO3,PO4,CO2
3259	1	ROS	091814	1210	EN	66 59.9 N	031 13.3 W	GPS	353	3	13	CTD,LADCP,O2,SiO3,PO4,CO2
3260	1	ROS	091814	1323	BE	66 55.0 N	030 49.8 W	GPS	589	9	14	CTD,LADCP,O2,SiO3,PO4,CO2
3260	1	ROS	091814	1338	BO	66 55.0 N	030 49.8 W	GPS	589	9	14	CTD,LADCP,O2,SiO3,PO4,CO2
3260	1	ROS	091814	1400	EN	66 55.0 N	030 49.8 W	GPS	589	9	14	CTD,LADCP,O2,SiO3,PO4,CO2
3261	1	ROS	091814	1517	BE	66 50.0 N	030 27.0 W	GPS	409	1	14	CTD,LADCP,O2,SiO3,PO4,CO2
3261	1	ROS	091814	1530	BO	66 50.0 N	030 26.9 W	GPS	409	1	14	CTD,LADCP,O2,SiO3,PO4,CO2

3261	1	ROS	091814	1550	EN	66 50.1 N	030 27.4 W	GPS	409	1	14	CTD,LADCP,O2,SiO3,PO4,CO2
3262	1	ROS	091814	1713	BE	66 45.1 N	030 02.9 W	GPS	328	4	12	CTD,LADCP,O2,SiO3,PO4,CO2
3262	1	ROS	091814	1722	BO	66 45.2 N	030 03.2 W	GPS	328	4	12	CTD,LADCP,O2,SiO3,PO4,CO2
3262	1	ROS	091814	1738	EN	66 45.4 N	030 03.3 W	GPS	328	4	12	CTD,LADCP,O2,SiO3,PO4,CO2
3263	1	ROS	091814	1900	BE	66 40.0 N	029 39.7 W	GPS	300	7	13	CTD,LADCP,O2,SiO3,PO4,CO2
3263	1	ROS	091814	1914	BO	66 39.9 N	029 38.8 W	GPS	300	7	13	CTD,LADCP,O2,SiO3,PO4,CO2
3263	1	ROS	091814	1932	EN	66 39.9 N	029 38.9 W	GPS	300	7	13	CTD,LADCP,O2,SiO3,PO4,CO2
3264	1	ROS	091814	2044	BE	66 35.1 N	029 16.9 W	GPS	309	5	12	CTD,LADCP,O2,SiO3,PO4,CO2
3264	1	ROS	091814	2104	BO	66 35.0 N	029 16.3 W	GPS	309	5	12	CTD,LADCP,O2,SiO3,PO4,CO2
3264	1	ROS	091814	2121	EN	66 35.0 N	029 16.5 W	GPS	309	5	12	CTD,LADCP,O2,SiO3,PO4,CO2
3265	1	ROS	091814	2235	BE	66 30.1 N	028 54.8 W	GPS	320	5	12	CTD,LADCP,O2,SiO3,PO4,CO2
3265	1	ROS	091814	2253	BO	66 30.0 N	028 54.4 W	GPS	320	5	12	CTD,LADCP,O2,SiO3,PO4,CO2
3265	1	ROS	091814	2313	EN	66 30.2 N	028 54.8 W	GPS	320	5	12	CTD,LADCP,O2,SiO3,PO4,CO2
3266	1	ROS	091914	0036	BE	66 25.2 N	028 31.9 W	GPS	297	3	11	CTD,LADCP,O2,SiO3,PO4,CO2
3266	1	ROS	091914	0050	BO	66 25.1 N	028 31.5 W	GPS	297	3	11	CTD,LADCP,O2,SiO3,PO4,CO2
3266	1	ROS	091914	0106	EN	66 25.1 N	028 31.7 W	GPS	297	3	11	CTD,LADCP,O2,SiO3,PO4,CO2
3267	1	ROS	091914	0225	BE	66 20.0 N	028 08.8 W	GPS	340	3	13	CTD,LADCP,O2,SiO3,PO4,CO2
3267	1	ROS	091914	0240	BO	66 19.9 N	028 08.4 W	GPS	340	3	13	CTD,LADCP,O2,SiO3,PO4,CO2
3267	1	ROS	091914	0258	EN	66 20.0 N	028 08.6 W	GPS	340	3	13	CTD,LADCP,O2,SiO3,PO4,CO2
3268	1	ROS	091914	0412	BE	66 15.0 N	027 46.3 W	GPS	471	1	17	CTD,LADCP,O2,SiO3,PO4,CO2
3268	1	ROS	091914	0432	BO	66 14.9 N	027 45.6 W	GPS	471	1	17	CTD,LADCP,O2,SiO3,PO4,CO2
3268	1	ROS	091914	0456	EN	66 15.0 N	027 45.4 W	GPS	471	1	17	CTD,LADCP,O2,SiO3,PO4,CO2
3269	1	ROS	091914	0550	BE	66 11.9 N	027 30.2 W	GPS	489	4	16	CTD,LADCP,O2,SiO3,PO4,CO2
3269	1	ROS	091914	0609	BO	66 12.0 N	027 30.0 W	GPS	489	4	16	CTD,LADCP,O2,SiO3,PO4,CO2
3269	1	ROS	091914	0634	EN	66 12.0 N	027 30.0 W	GPS	489	4	16	CTD,LADCP,O2,SiO3,PO4,CO2
3270	1	ROS	091914	0721	BE	66 09.0 N	027 15.3 W	GPS	520	3	13	CTD,LADCP,O2,SiO3,PO4,CO2
3270	1	ROS	091914	0738	BO	66 09.0 N	027 14.9 W	GPS	520	3	13	CTD,LADCP,O2,SiO3,PO4,CO2
3270	1	ROS	091914	0757	EN	66 08.9 N	027 14.9 W	GPS	520	3	13	CTD,LADCP,O2,SiO3,PO4,CO2
3271	1	ROS	091914	0841	BE	66 05.1 N	027 03.2 W	GPS	657	4	13	CTD,LADCP,O2,SiO3,PO4,CO2
3271	1	ROS	091914	0902	BO	66 04.9 N	027 02.4 W	GPS	657	4	13	CTD,LADCP,O2,SiO3,PO4,CO2
3271	1	ROS	091914	0925	EN	66 04.8 N	027 01.8 W	GPS	657	4	13	CTD,LADCP,O2,SiO3,PO4,CO2
3272	1	ROS	091914	1010	BE	66 01.1 N	026 48.3 W	GPS	442	3	10	CTD,LADCP,O2,SiO3,PO4,CO2
3272	1	ROS	091914	1027	BO	66 00.9 N	026 47.7 W	GPS	442	3	10	CTD,LADCP,O2,SiO3,PO4,CO2

3272	1	ROS	091914	1041	EN	66 00.9 N	026 47.5 W	GPS	442	3	10	CTD,LADCP,O2,SiO3,PO4,CO2
3273	1	ROS	091914	1143	BE	65 56.0 N	026 29.1 W	GPS	284	2	8	CTD,LADCP,O2,SiO3,PO4,CO2
3273	1	ROS	091914	1157	BO	65 55.9 N	026 29.0 W	GPS	284	2	8	CTD,LADCP,O2,SiO3,PO4,CO2
3273	1	ROS	091914	1210	EN	65 55.8 N	026 29.2 W	GPS	284	2	8	CTD,LADCP,O2,SiO3,PO4,CO2
3274	1	ROS	091914	1335	BE	65 49.9 N	026 00.0 W	GPS	220	2	8	CTD,LADCP,O2,SiO3,PO4,CO2
3274	1	ROS	091914	1346	BO	65 49.8 N	025 59.6 W	GPS	220	2	8	CTD,LADCP,O2,SiO3,PO4,CO2
3274	1	ROS	091914	1356	EN	65 49.7 N	025 59.5 W	GPS	220	2	8	CTD,LADCP,O2,SiO3,PO4,CO2
3275	1	ROS	091914	1505	BE	65 45.0 N	025 38.6 W	GPS	271	3	9	CTD,LADCP,O2,SiO3,PO4,CO2
3275	1	ROS	091914	1515	BO	65 45.0 N	025 38.5 W	GPS	271	3	9	CTD,LADCP,O2,SiO3,PO4,CO2
3275	1	ROS	091914	1527	EN	65 45.0 N	025 38.5 W	GPS	271	3	9	CTD,LADCP,O2,SiO3,PO4,CO2
3276	1	ROS	091914	1636	BE	65 40.0 N	025 15.9 W	GPS	88	3	5	CTD,LADCP,O2,SiO3,PO4,CO2
3276	1	ROS	091914	1643	BO	65 40.0 N	025 15.8 W	GPS	88	3	5	CTD,LADCP,O2,SiO3,PO4,CO2
3276	1	ROS	091914	1648	EN	65 40.0 N	025 15.8 W	GPS	88	3	5	CTD,LADCP,O2,SiO3,PO4,CO2
3277	1	ROS	091914	1752	BE	65 35.1 N	024 55.4 W	GPS	67	3	5	CTD,LADCP,O2,SiO3,PO4,CO2
3277	1	ROS	091914	1804	BO	65 34.8 N	024 54.8 W	GPS	67	3	5	CTD,LADCP,O2,SiO3,PO4,CO2
3277	1	ROS	091914	1810	EN	65 34.8 N	024 54.8 W	GPS	67	3	5	CTD,LADCP,O2,SiO3,PO4,CO2
3278	1	ROS	092114	0825	BE	64 24.5 N	014 03.2 W	GPS	107	4	6	CTD,LADCP,O2,SiO3,PO4,CO2
3278	1	ROS	092114	0835	BO	64 24.6 N	014 02.7 W	GPS	107	4	6	CTD,LADCP,O2,SiO3,PO4,CO2
3278	1	ROS	092114	0843	EN	64 24.7 N	014 02.5 W	GPS	107	4	6	CTD,LADCP,O2,SiO3,PO4,CO2
3279	1	ROS	092114	1011	BE	64 17.0 N	013 36.1 W	GPS	161	2	8	CTD,LADCP,O2,SiO3,PO4,CO2
3279	1	ROS	092114	1021	BO	64 16.9 N	013 35.8 W	GPS	161	2	8	CTD,LADCP,O2,SiO3,PO4,CO2
3279	1	ROS	092114	1030	EN	64 17.0 N	013 35.7 W	GPS	161	2	8	CTD,LADCP,O2,SiO3,PO4,CO2
3280	1	ROS	092114	1116	BE	64 14.1 N	013 21.3 W	GPS	174	4	9	CTD,LADCP,O2,SiO3,PO4,CO2
3280	1	ROS	092114	1126	BO	64 14.0 N	013 20.7 W	GPS	174	4	9	CTD,LADCP,O2,SiO3,PO4,CO2
3280	1	ROS	092114	1140	EN	64 13.8 N	013 20.6 W	GPS	174	4	9	CTD,LADCP,O2,SiO3,PO4,CO2
3281	1	ROS	092114	1243	BE	64 08.0 N	013 03.0 W	GPS	168	3	9	CTD,LADCP,O2,SiO3,PO4,CO2
3281	1	ROS	092114	1252	BO	64 07.9 N	013 02.8 W	GPS	168	3	9	CTD,LADCP,O2,SiO3,PO4,CO2
3281	1	ROS	092114	1302	EN	64 07.8 N	013 02.9 W	GPS	168	3	9	CTD,LADCP,O2,SiO3,PO4,CO2
3282	1	ROS	092114	1344	BE	64 05.0 N	012 52.1 W	GPS	576	4	13	CTD,LADCP,O2,SiO3,PO4,CO2
3282	1	ROS	092114	1358	BO	64 05.0 N	012 51.8 W	GPS	576	4	13	CTD,LADCP,O2,SiO3,PO4,CO2
3282	1	ROS	092114	1421	EN	64 05.0 N	012 51.8 W	GPS	576	4	13	CTD,LADCP,O2,SiO3,PO4,CO2
3283	1	ROS	092114	1517	BE	64 01.0 N	012 38.0 W	GPS	566	2	13	CTD,LADCP,O2,SiO3,PO4,CO2
3283	1	ROS	092114	1532	BO	64 01.0 N	012 38.1 W	GPS	566	2	13	CTD,LADCP,O2,SiO3,PO4,CO2

3283	1	ROS	092114	1552	EN	64 01.0 N	012 38.2 W	GPS	566	2	13	CTD,LADCP,O2,SiO3,PO4,CO2
3284	1	ROS	092114	1656	BE	63 57.0 N	012 20.0 W	GPS	458	2	12	CTD,LADCP,O2,SiO3,PO4,CO2
3284	1	ROS	092114	1710	BO	63 57.0 N	012 19.7 W	GPS	458	2	12	CTD,LADCP,O2,SiO3,PO4,CO2
3284	1	ROS	092114	1728	EN	63 57.1 N	012 19.4 W	GPS	458	2	12	CTD,LADCP,O2,SiO3,PO4,CO2
3285	1	ROS	092114	1842	BE	63 50.3 N	012 00.6 W	GPS	385	4	14	CTD,LADCP,O2,SiO3,PO4,CO2
3285	1	ROS	092114	1858	BO	63 50.0 N	011 59.7 W	GPS	385	4	14	CTD,LADCP,O2,SiO3,PO4,CO2
3285	1	ROS	092114	1916	EN	63 50.2 N	011 59.2 W	GPS	385	4	14	CTD,LADCP,O2,SiO3,PO4,CO2
3286	1	ROS	092114	2025	BE	63 44.3 N	011 40.7 W	GPS	346	6	13	CTD,LADCP,O2,SiO3,PO4,CO2
3286	1	ROS	092114	2043	BO	63 44.1 N	011 39.4 W	GPS	346	6	13	CTD,LADCP,O2,SiO3,PO4,CO2
3286	1	ROS	092114	2101	EN	63 44.2 N	011 38.5 W	GPS	346	6	13	CTD,LADCP,O2,SiO3,PO4,CO2
3287	1	ROS	092114	2229	BE	63 36.1 N	011 15.6 W	GPS	302	4	12	CTD,LADCP,O2,SiO3,PO4,CO2
3287	1	ROS	092114	2244	BO	63 36.0 N	011 14.9 W	GPS	302	4	12	CTD,LADCP,O2,SiO3,PO4,CO2
3287	1	ROS	092114	2259	EN	63 36.0 N	011 14.7 W	GPS	302	4	12	CTD,LADCP,O2,SiO3,PO4,CO2
3288	1	ROS	092214	0033	BE	63 29.0 N	010 49.2 W	GPS	441	3	15	CTD,LADCP,O2,SiO3,PO4,CO2
3288	1	ROS	092214	0048	BO	63 28.9 N	010 49.0 W	GPS	441	3	15	CTD,LADCP,O2,SiO3,PO4,CO2
3288	1	ROS	092214	0107	EN	63 28.9 N	010 49.2 W	GPS	441	3	15	CTD,LADCP,O2,SiO3,PO4,CO2
3289	1	ROS	092214	0249	BE	63 20.1 N	010 25.4 W	GPS	328	4	11	CTD,LADCP,O2,SiO3,PO4,CO2
3289	1	ROS	092214	0302	BO	63 20.0 N	010 24.9 W	GPS	328	4	11	CTD,LADCP,O2,SiO3,PO4,CO2
3289	1	ROS	092214	0317	EN	63 20.1 N	010 24.7 W	GPS	328	4	11	CTD,LADCP,O2,SiO3,PO4,CO2
3290	1	ROS	092214	0500	BE	63 14.1 N	009 58.3 W	GPS	485	3	15	CTD,LADCP,O2,SiO3,PO4,CO2
3290	1	ROS	092214	0516	BO	63 14.0 N	009 57.6 W	GPS	485	3	15	CTD,LADCP,O2,SiO3,PO4,CO2
3290	1	ROS	092214	0538	EN	63 14.0 N	009 57.4 W	GPS	485	3	15	CTD,LADCP,O2,SiO3,PO4,CO2
3291	1	ROS	092214	0704	BE	63 06.0 N	009 38.0 W	GPS	492	1	13	CTD,LADCP,O2,SiO3,PO4,CO2
3291	1	ROS	092214	0719	BO	63 05.9 N	009 37.6 W	GPS	492	1	13	CTD,LADCP,O2,SiO3,PO4,CO2
3291	1	ROS	092214	0738	EN	63 05.9 N	009 37.2 W	GPS	492	1	13	CTD,LADCP,O2,SiO3,PO4,CO2
3292	1	ROS	092214	0911	BE	62 58.0 N	009 09.1 W	GPS	444	1	12	CTD,LADCP,O2,SiO3,PO4,CO2
3292	1	ROS	092214	0929	BO	62 58.1 N	009 08.4 W	GPS	444	1	12	CTD,LADCP,O2,SiO3,PO4,CO2
3292	1	ROS	092214	0949	EN	62 58.2 N	009 07.9 W	GPS	444	1	12	CTD,LADCP,O2,SiO3,PO4,CO2
3293	1	ROS	092214	1101	BE	62 51.0 N	008 50.3 W	GPS	461	4	13	CTD,LADCP,O2,SiO3,PO4,CO2
3293	1	ROS	092214	1118	BO	62 50.9 N	008 50.0 W	GPS	461	4	13	CTD,LADCP,O2,SiO3,PO4,CO2
3293	1	ROS	092214	1136	EN	62 50.8 N	008 50.1 W	GPS	461	4	13	CTD,LADCP,O2,SiO3,PO4,CO2
3294	1	ROS	092214	1302	BE	62 44.0 N	008 27.1 W	GPS	479	2	11	CTD,LADCP,O2,SiO3,PO4,CO2
3294	1	ROS	092214	1317	BO	62 43.9 N	008 27.2 W	GPS	479	2	11	CTD,LADCP,O2,SiO3,PO4,CO2

3294	1	ROS	092214	1337	EN	62 43.9 N	008 27.6 W	GPS	479	2	11	CTD,LADCP,O2,SiO3,PO4,CO2
3295	1	ROS	092214	1517	BE	62 35.0 N	008 02.0 W	GPS	412	3	12	CTD,LADCP,O2,SiO3,PO4,CO2
3295	1	ROS	092214	1530	BO	62 34.9 N	008 02.3 W	GPS	412	3	12	CTD,LADCP,O2,SiO3,PO4,CO2
3295	1	ROS	092214	1545	EN	62 35.0 N	008 02.6 W	GPS	412	3	12	CTD,LADCP,O2,SiO3,PO4,CO2
3296	1	ROS	092214	1724	BE	62 26.1 N	007 39.0 W	GPS	102	4	6	CTD,LADCP,O2,SiO3,PO4,CO2
3296	1	ROS	092214	1732	BO	62 26.0 N	007 38.9 W	GPS	102	4	6	CTD,LADCP,O2,SiO3,PO4,CO2
3296	1	ROS	092214	1740	EN	62 26.0 N	007 39.0 W	GPS	102	4	6	CTD,LADCP,O2,SiO3,PO4,CO2
3297	1	ROS	092214	1905	BE	62 20.2 N	007 15.4 W	GPS	92	3	4	CTD,LADCP,O2,SiO3,PO4,CO2
3297	1	ROS	092214	1916	BO	62 20.0 N	007 14.7 W	GPS	92	3	4	CTD,LADCP,O2,SiO3,PO4,CO2
3297	1	ROS	092214	1922	EN	62 20.0 N	007 14.5 W	GPS	92	3	4	CTD,LADCP,O2,SiO3,PO4,CO2
3298	1	ROS	092314	0128	BE	61 50.2 N	006 21.9 W	GPS	77	6	4	CTD,LADCP,O2,SiO3,PO4,CO2
3298	1	ROS	092314	0139	BO	61 49.8 N	006 22.1 W	GPS	77	6	4	CTD,LADCP,O2,SiO3,PO4,CO2
3298	1	ROS	092314	0144	EN	61 49.8 N	006 22.2 W	GPS	77	6	4	CTD,LADCP,O2,SiO3,PO4,CO2
3299	1	ROS	092314	0312	BE	61 42.7 N	005 58.0 W	GPS	292	3	11	CTD,LADCP,O2,SiO3,PO4,CO2
3299	1	ROS	092314	0327	BO	61 42.4 N	005 57.6 W	GPS	292	3	11	CTD,LADCP,O2,SiO3,PO4,CO2
3299	1	ROS	092314	0341	EN	61 42.3 N	005 57.7 W	GPS	292	3	11	CTD,LADCP,O2,SiO3,PO4,CO2
3300	1	ROS	092314	0455	BE	61 37.1 N	005 36.4 W	GPS	316	4	13	CTD,LADCP,O2,SiO3,PO4,CO2
3300	1	ROS	092314	0508	BO	61 36.9 N	005 36.0 W	GPS	316	4	13	CTD,LADCP,O2,SiO3,PO4,CO2
3300	1	ROS	092314	0525	EN	61 36.9 N	005 35.8 W	GPS	316	4	13	CTD,LADCP,O2,SiO3,PO4,CO2
3301	1	ROS	092314	0633	BE	61 31.0 N	005 18.9 W	GPS	288	4	10	CTD,LADCP,O2,SiO3,PO4,CO2
3301	1	ROS	092314	0644	BO	61 30.9 N	005 18.9 W	GPS	288	4	10	CTD,LADCP,O2,SiO3,PO4,CO2
3301	1	ROS	092314	0657	EN	61 31.0 N	005 18.9 W	GPS	288	4	10	CTD,LADCP,O2,SiO3,PO4,CO2
3302	1	ROS	092314	0807	BE	61 25.1 N	005 01.2 W	GPS	223	4	10	CTD,LADCP,O2,SiO3,PO4,CO2
3302	1	ROS	092314	0818	BO	61 25.0 N	005 00.9 W	GPS	223	4	10	CTD,LADCP,O2,SiO3,PO4,CO2
3302	1	ROS	092314	0831	EN	61 24.9 N	005 00.7 W	GPS	223	4	10	CTD,LADCP,O2,SiO3,PO4,CO2
3303	1	ROS	092314	0934	BE	61 20.0 N	004 43.0 W	GPS	739	3	16	CTD,LADCP,O2,SiO3,PO4,CO2
3303	1	ROS	092314	0953	BO	61 19.9 N	004 42.7 W	GPS	739	3	16	CTD,LADCP,O2,SiO3,PO4,CO2
3303	1	ROS	092314	1018	EN	61 19.8 N	004 42.5 W	GPS	739	3	16	CTD,LADCP,O2,SiO3,PO4,CO2
3304	1	ROS	092314	1111	BE	61 16.0 N	004 28.2 W	GPS	1054	3	18	CTD,LADCP,O2,SiO3,PO4,CO2
3304	1	ROS	092314	1137	BO	61 15.9 N	004 27.8 W	GPS	1054	3	18	CTD,LADCP,O2,SiO3,PO4,CO2
3304	1	ROS	092314	1212	EN	61 15.7 N	004 27.3 W	GPS	1054	3	18	CTD,LADCP,O2,SiO3,PO4,CO2
3305	1	ROS	092314	1253	BE	61 12.0 N	004 17.9 W	GPS	1077	3	19	CTD,LADCP,O2,SiO3,PO4,CO2
3305	1	ROS	092314	1316	BO	61 11.9 N	004 17.8 W	GPS	1077	3	19	CTD,LADCP,O2,SiO3,PO4,CO2

3305	1	ROS	092314	1347	EN	61 11.8 N	004 17.5 W	GPS	1077	3	19	CTD,LADCP,O2,SiO3,PO4,CO2
3306	1	ROS	092314	1441	BE	61 08.0 N	004 03.9 W	GPS	1122	2	19	CTD,LADCP,O2,SiO3,PO4,CO2
3306	1	ROS	092314	1506	BO	61 07.8 N	004 04.1 W	GPS	1122	2	19	CTD,LADCP,O2,SiO3,PO4,CO2
3306	1	ROS	092314	1542	EN	61 07.7 N	004 04.5 W	GPS	1122	2	19	CTD,LADCP,O2,SiO3,PO4,CO2
3307	1	ROS	092314	1633	BE	61 03.9 N	003 52.0 W	GPS	1146	2	21	CTD,LADCP,O2,SiO3,PO4,CO2
3307	1	ROS	092314	1657	BO	61 03.8 N	003 51.9 W	GPS	1146	2	21	CTD,LADCP,O2,SiO3,PO4,CO2
3307	1	ROS	092314	1732	EN	61 03.6 N	003 52.1 W	GPS	1146	2	21	CTD,LADCP,O2,SiO3,PO4,CO2
3308	1	ROS	092314	1825	BE	60 59.1 N	003 38.2 W	GPS	1102	5	19	CTD,LADCP,O2,SiO3,PO4,CO2
3308	1	ROS	092314	1857	BO	60 58.9 N	003 37.7 W	GPS	1102	5	19	CTD,LADCP,O2,SiO3,PO4,CO2
3308	1	ROS	092314	1957	EN	60 58.8 N	003 37.3 W	GPS	1102	5	19	CTD,LADCP,O2,SiO3,PO4,CO2
3308	2	ROS	092314	2035	BE	60 59.0 N	003 37.9 W	GPS	1103	3	-	CTD,LADCP,O2,SiO3,PO4,CO2
3308	2	ROS	092314	2059	BO	60 59.0 N	003 37.7 W	GPS	1103	3	-	CTD,LADCP,O2,SiO3,PO4,CO2
3308	2	ROS	092314	2119	EN	60 59.0 N	003 37.6 W	GPS	1103	3	-	CTD,LADCP,O2,SiO3,PO4,CO2
3309	1	ROS	092314	2234	BE	60 52.2 N	003 18.4 W	GPS	681	5	16	CTD,LADCP,O2,SiO3,PO4,CO2
3309	1	ROS	092314	2255	BO	60 52.0 N	003 17.8 W	GPS	681	5	16	CTD,LADCP,O2,SiO3,PO4,CO2
3309	1	ROS	092314	2321	EN	60 52.0 N	003 17.6 W	GPS	681	5	16	CTD,LADCP,O2,SiO3,PO4,CO2
3310	1	ROS	092414	0050	BE	60 45.1 N	002 55.4 W	GPS	352	5	12	CTD,LADCP,O2,SiO3,PO4,CO2
3310	1	ROS	092414	0104	BO	60 44.9 N	002 55.0 W	GPS	352	5	12	CTD,LADCP,O2,SiO3,PO4,CO2
3310	1	ROS	092414	0121	EN	60 44.9 N	002 54.7 W	GPS	352	5	12	CTD,LADCP,O2,SiO3,PO4,CO2
3311	1	ROS	092414	0231	BE	60 39.0 N	002 37.8 W	GPS	135	4	7	CTD,LADCP,O2,SiO3,PO4,CO2
3311	1	ROS	092414	0253	BO	60 38.2 N	002 37.1 W	GPS	135	4	7	CTD,LADCP,O2,SiO3,PO4,CO2
3311	1	ROS	092414	0302	EN	60 38.3 N	002 37.2 W	GPS	135	4	7	CTD,LADCP,O2,SiO3,PO4,CO2
3312	1	ROS	092414	0432	BE	60 31.2 N	002 16.2 W	GPS	139	5	7	CTD,LADCP,O2,SiO3,PO4,CO2
3312	1	ROS	092414	0443	BO	60 31.0 N	002 16.0 W	GPS	139	5	7	CTD,LADCP,O2,SiO3,PO4,CO2
3312	1	ROS	092414	0453	EN	60 31.0 N	002 16.0 W	GPS	139	5	7	CTD,LADCP,O2,SiO3,PO4,CO2
3313	1	ROS	092414	0610	BE	60 25.1 N	001 55.0 W	GPS	112	4	7	CTD,LADCP,O2,SiO3,PO4,CO2
3313	1	ROS	092414	0619	BO	60 25.0 N	001 55.0 W	GPS	112	4	7	CTD,LADCP,O2,SiO3,PO4,CO2
3313	1	ROS	092414	0628	EN	60 25.0 N	001 54.9 W	GPS	112	4	7	CTD,LADCP,O2,SiO3,PO4,CO2

Table 2

	O ₂ , ml/l	Silicate, μMol kg ⁻¹	Phosphate, μMol kg ⁻¹
Total amount of analyzed samples	1060	1147	1157
Number of duplicates	70	151	161
Mean difference of duplicates	0.01	0.03	0.01
Min difference of duplicates	0.00	0.00	0.00
Max difference of duplicates	0.02	0.09	0.05
Median difference of duplicates	0.005	0.022	0.007
Standard deviation of difference	0.007	0.023	0.008
Accuracy	0.106%	0.460%	1.067%

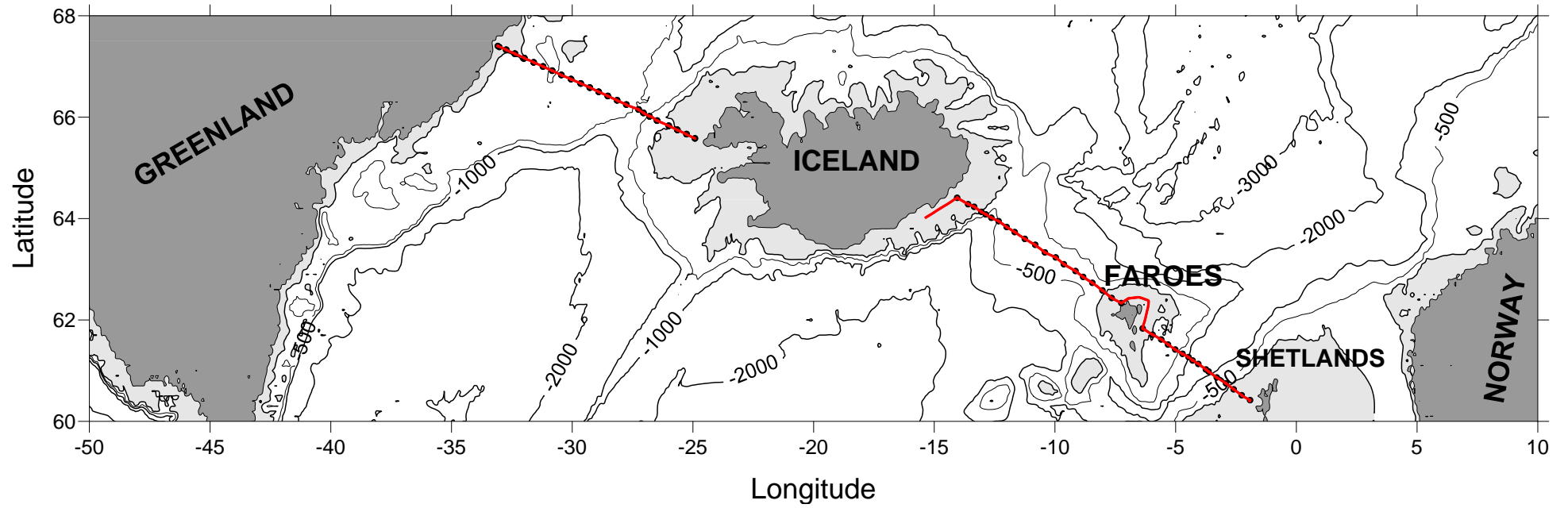


Fig. 1 Station locations (black circles) and ship track (in red). The shelf area with depth less than 200 m is shaded.

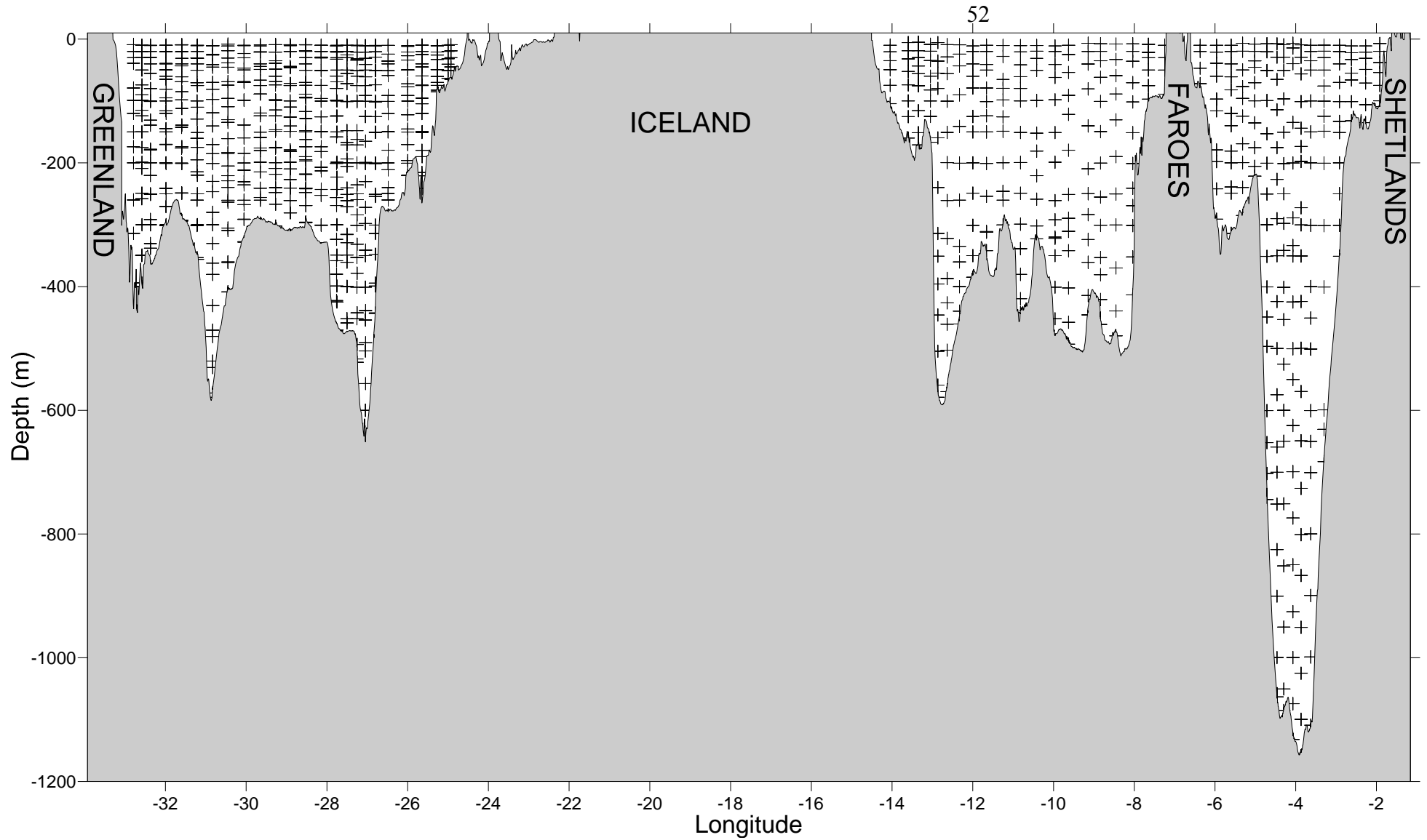


Figure 2. Vertical distribution of samples along the sill sections.

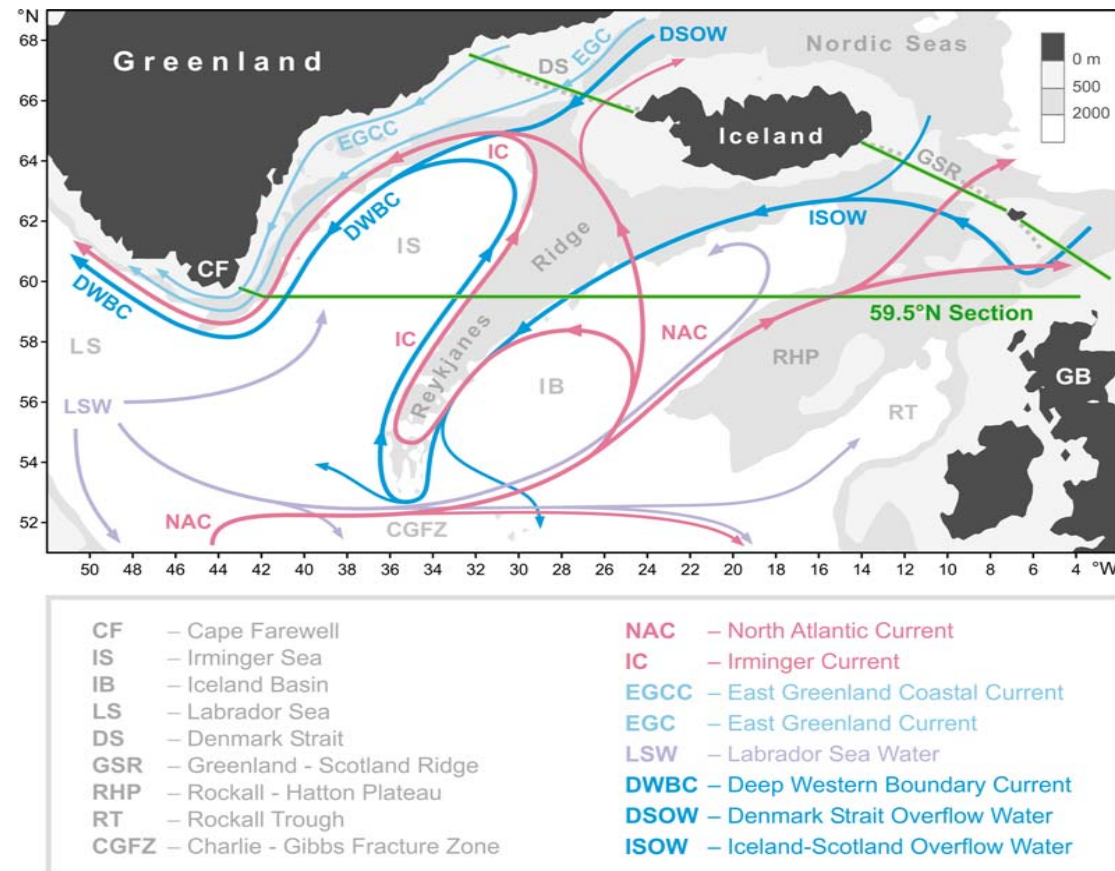


Figure 3. Schematic diagram of the large-scale circulation in the northern North Atlantic compiled from [Schmitz and McCartney, 1993; Schott and Brandt, 2007; Sutherland and Pickart, 2008; Lherminier et al., 2010]. Abbreviations for the main topographic features, currents and water masses are explained in the legend. The nominal locations of the 59.5°N hydrographic section (1997 – present) and sections across the straits between Greenland, Iceland, Faeroe and Shetland Islands (2011 – present) are shown with the solid green lines.

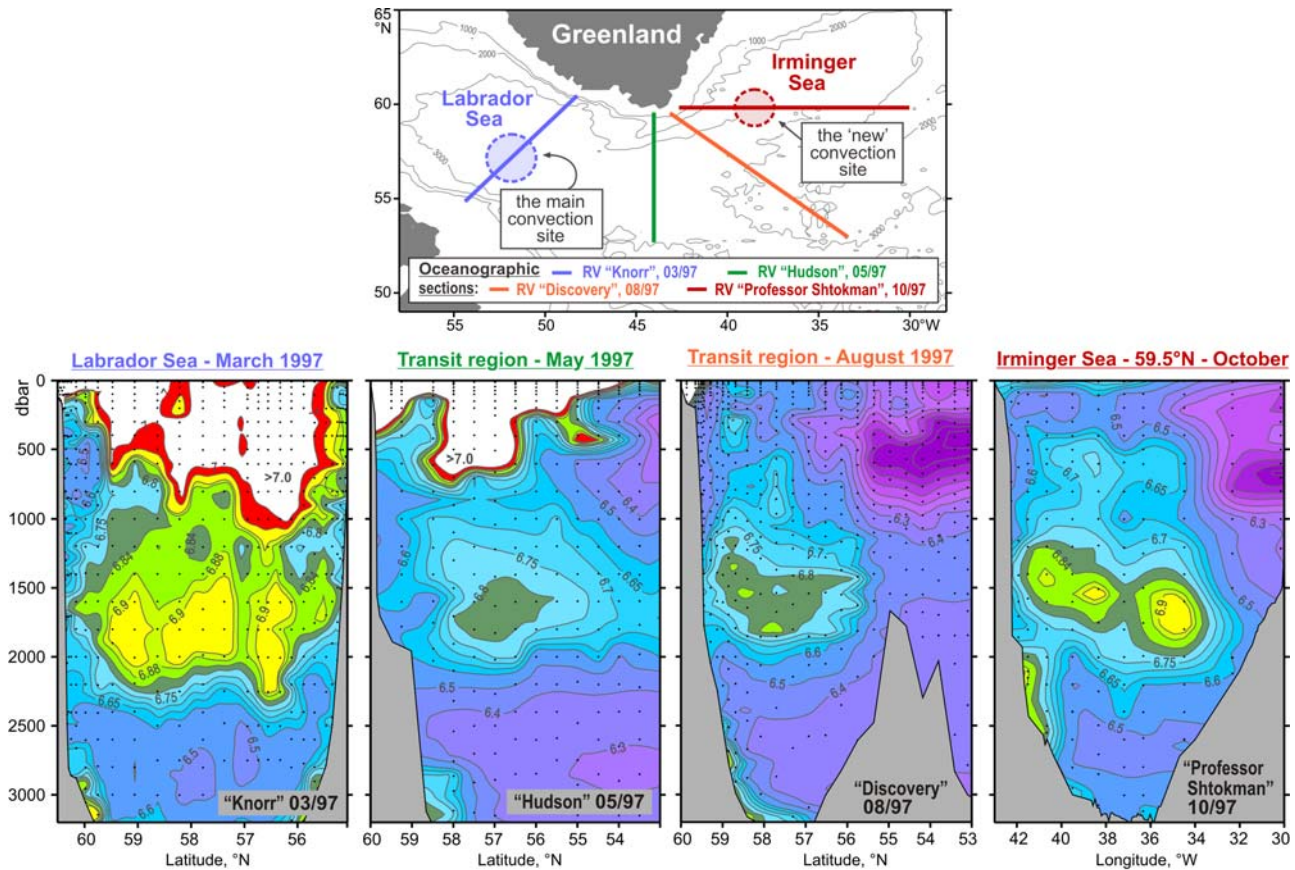


Figure 4. Oxygen concentrations (ml/l) in the water column (lower panel) as observed in March–October 1997 in four hydrographic sections (upper panel) ending nearby the southern tip of Greenland. A separate oxygen maximum in the LSW layer (1000–2000 m) in the Irminger Sea at 59.5°N strongly implies local convective renewal of LSW before 1997. Adapted from [Falina et al., 2007].

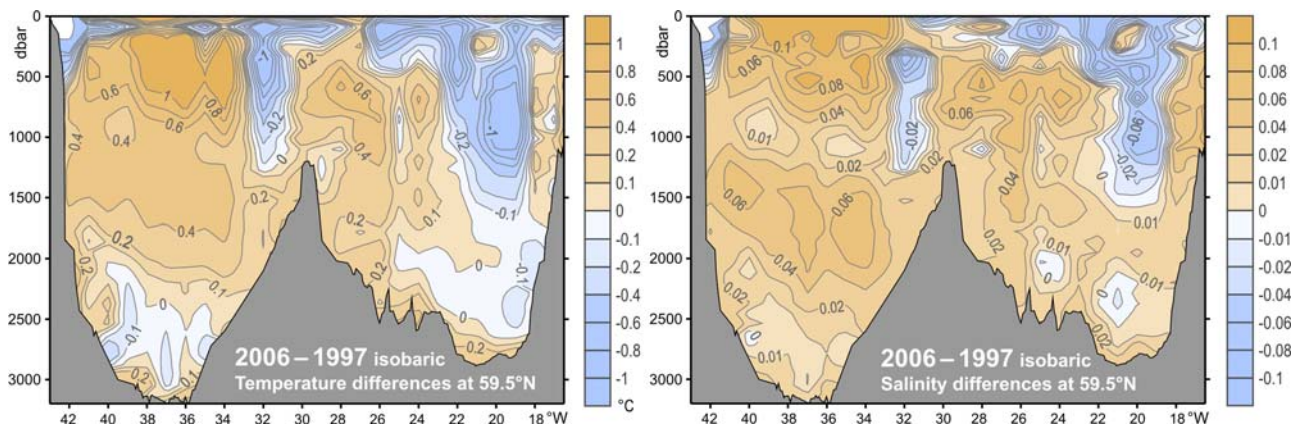


Figure 5. Warming and salinification in the northern North Atlantic between the mid-1990s and mid-2000s, as observed at 59.5°N. The figure shows the 2006–1997 temperature (°C, left) and salinity (right) differences on isobaric surfaces in the Irminger Sea and Iceland Basin. Adapted from [Sarafanov et al., 2007].

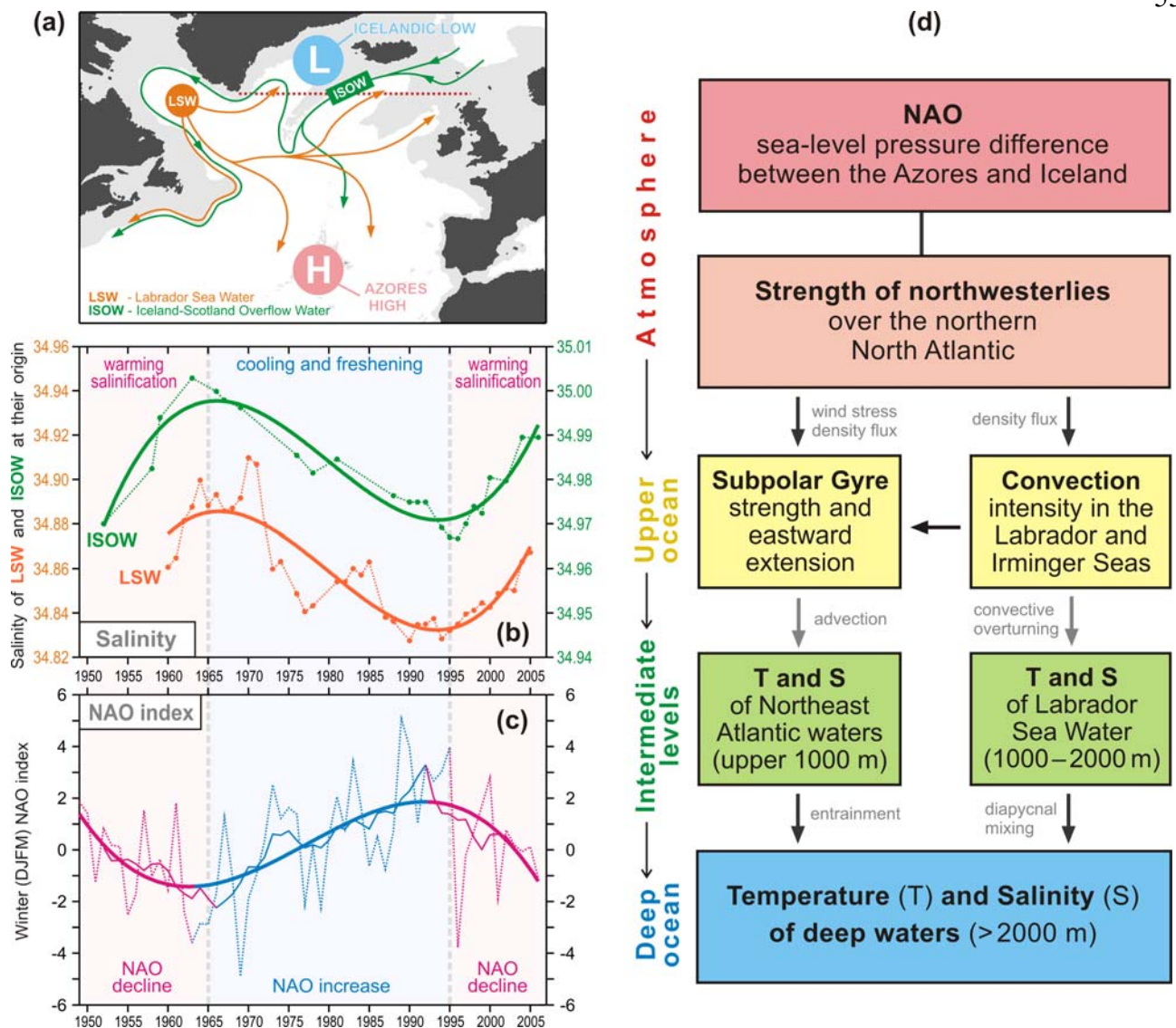


Figure 6. Coherence of the decadal salinity changes (1950s – 2000s) of the intermediate (LSW) and deep (ISOW) waters in the northern North Atlantic and their link to the North Atlantic Oscillation (NAO) index. **(a)** Schematic representation of the LSW and ISOW pathways and locations of the Icelandic Low (L) and Azores High (H) centers constituting the NAO dipole pattern. The red dotted line indicates the 59.5°N transatlantic section. **(b)** Salinity time series for LSW in the Labrador Sea [Yashayaev, 2007] and ISOW in the Iceland basin [Boessenkool et al., 2007; Sarafanov et al., 2007] overlaid by the third order polynomial fits. **(c)** Time series of the winter NAO index, after [Hurrell, 1995], overlaid by 7-year running mean and third order polynomial fit. **(d)** Mechanism of the NAO effect on the decadal changes in temperature (T) and salinity (S) of the northern North Atlantic intermediate and deep waters. Positive / negative links shown with the dark / light grey arrows mean that changes in ‘causative’ and ‘consequential’ characteristics have the same / opposite sign(s). The overall effect of the NAO on T and S of the in the water column is negative: persistent NAO decline leads to warming and salinification of the water masses and vice versa, as shown in (b) and (c). Adapted from [Sarafanov, 2009].

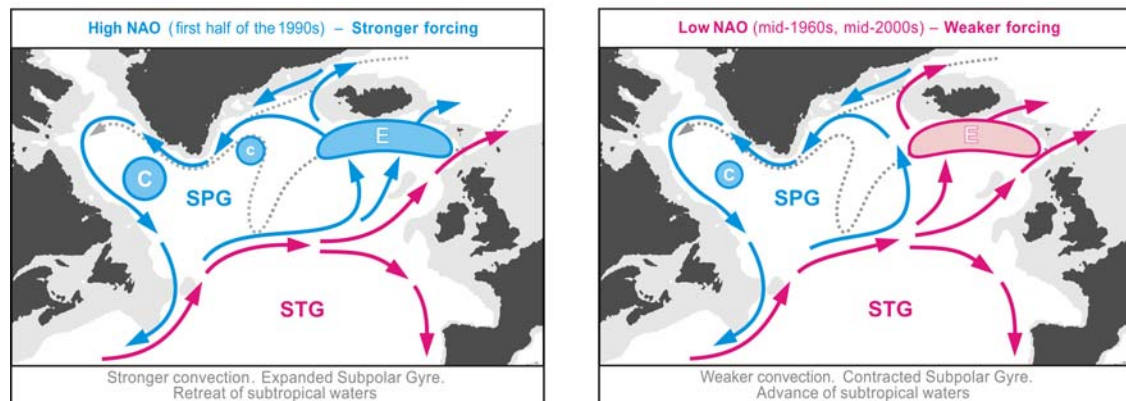


Figure 7. Schematic representation of the upper-ocean circulation and convection intensity in the northern North Atlantic under high (left) and low (right) NAO conditions. Blue (magenta) solid arrows indicate the upper-ocean flows with higher fraction of colder fresher subpolar (warmer saltier subtropical) waters. The main pathways of the Nordic overflow-derived deep waters are shown with the dotted curves. “C” and “E” symbols are used to denote, respectively, the deep convection sites and the domain, where the Atlantic waters are entrained into ISOW. Larger (smaller) circles indicate stronger (weaker) convection. SPG and STG – the subpolar and subtropical gyres, respectively. Adapted from [Sarafanov, 2009].

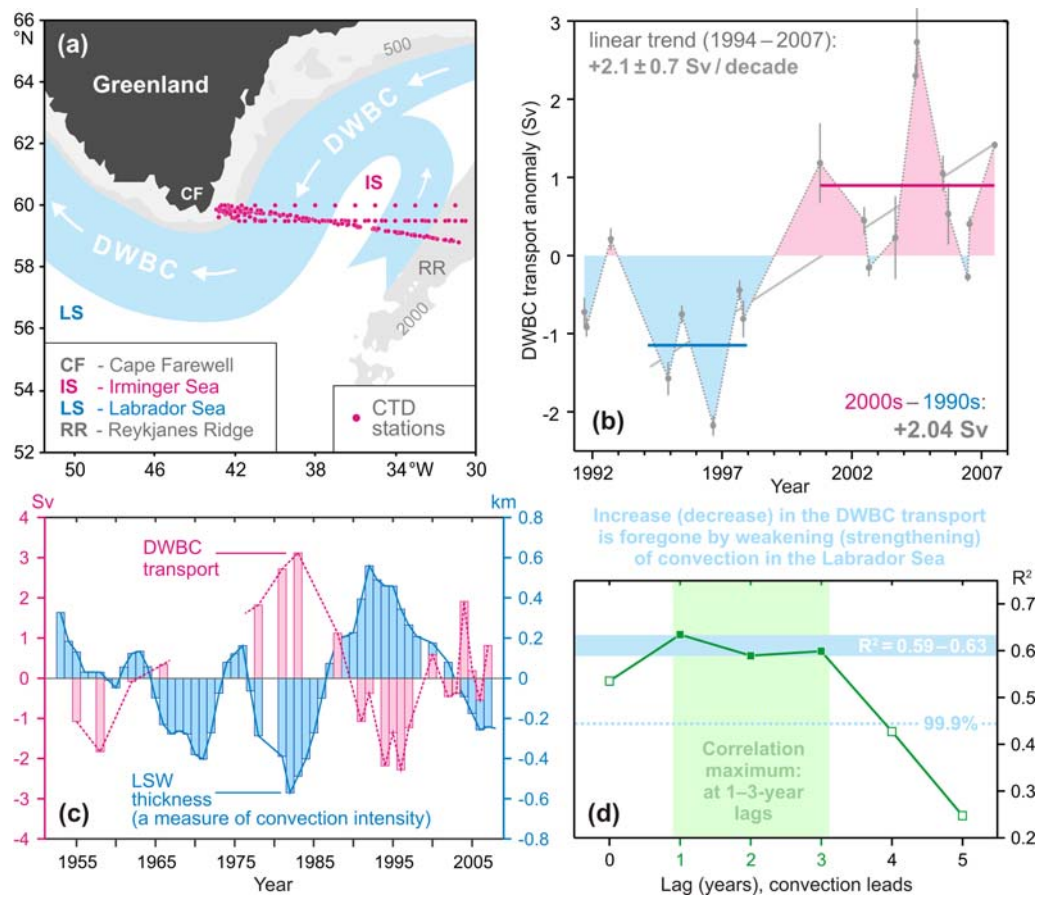


Figure 8. The Deep Western Boundary Current (DWBC) transport variability and its link to the convection intensity in the Labrador Sea. **(a)** Locations of the hydrographic sections (1991–2007) and schematic of the deep water circulation in the Irminger Sea. **(b)** The DWBC transport anomalies at Cape Farewell in 1991–2007, $1 \text{ Sv} = 10^6 \text{ m}^3 \text{ s}^{-1}$. The 1994–1997 and 2000–2007 mean anomalies and the 1994–2007 linear trend are shown. **(c)** Anomalies of the DWBC transport at Cape Farewell and the Labrador Sea Water (LSW) thickness in the Labrador Sea in the 1950s–2000s. **(d)** Correlation coefficient (R^2) for the two time series shown in (c) at the 0–5-year lag, the LSW thickness leads. The correlation maximum is achieved at the 1–3-year lag. The DWBC transport anomalies in the southern Irminger Sea are foregone by the convection intensity anomalies in the Labrador Sea. Adapted from [Sarafanov et al., 2009].

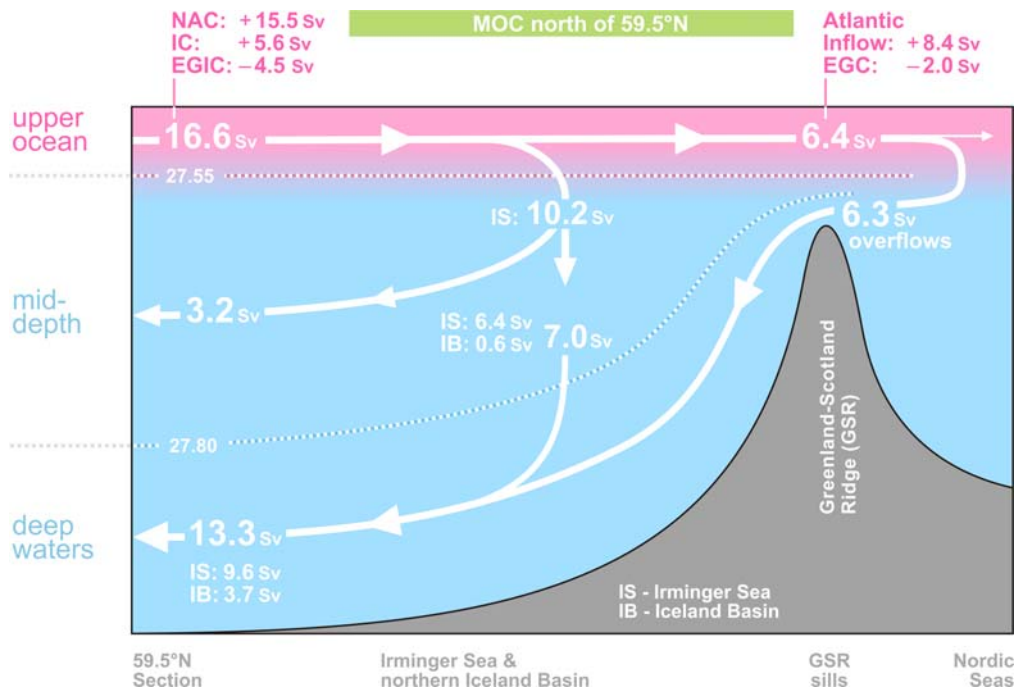


Figure 9. Schematic diagram of the Meridional Overturning Circulation (MOC) at the northern periphery of the Atlantic Ocean, northeast of Cape Farewell. The dotted lines refer to the σ_0 isopycnals 27.55 and 27.80. The arrows denote the integral meridional and diapycnal volume fluxes. Where the signs are specified, the positive (negative) transports are northward (southward). The NAC and EGIC transports in the upper layer ($\sigma_0 < 27.55$) at 59.5°N are the throughputs accounting for the recirculations. EGIC – the East Greenland / Irminger Current – refers to the upper part of the Western Boundary Current. Other abbreviations are explained in the legend to **Figure 3**. Adapted from [Sarafanov et al., 2012].

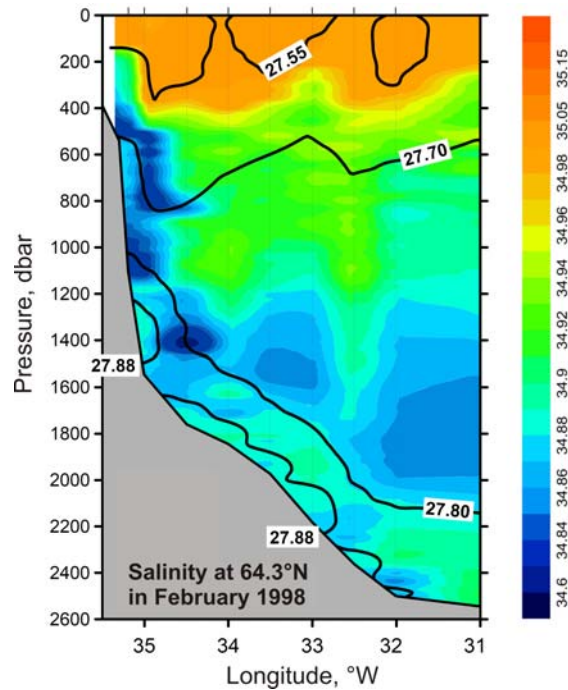


Figure 10. Salinity observed in the northwestern Irminger Sea at 64.3°N in February 1998. The σ_0 isopycnals 27.55, 27.70, 27.80 and 27.88 are plotted as the thick black lines; the station locations are marked with the ticks on the top axis. The plot shows fresh dense waters descending (cascading) down the continental slope of Greenland down to the LSW layer ($27.70 < \sigma_0 < 27.80$) and the layer of the Nordic Seas overflow-derived deep waters ($\sigma_0 > 27.80$). Adapted from [Falina et al., 2012].

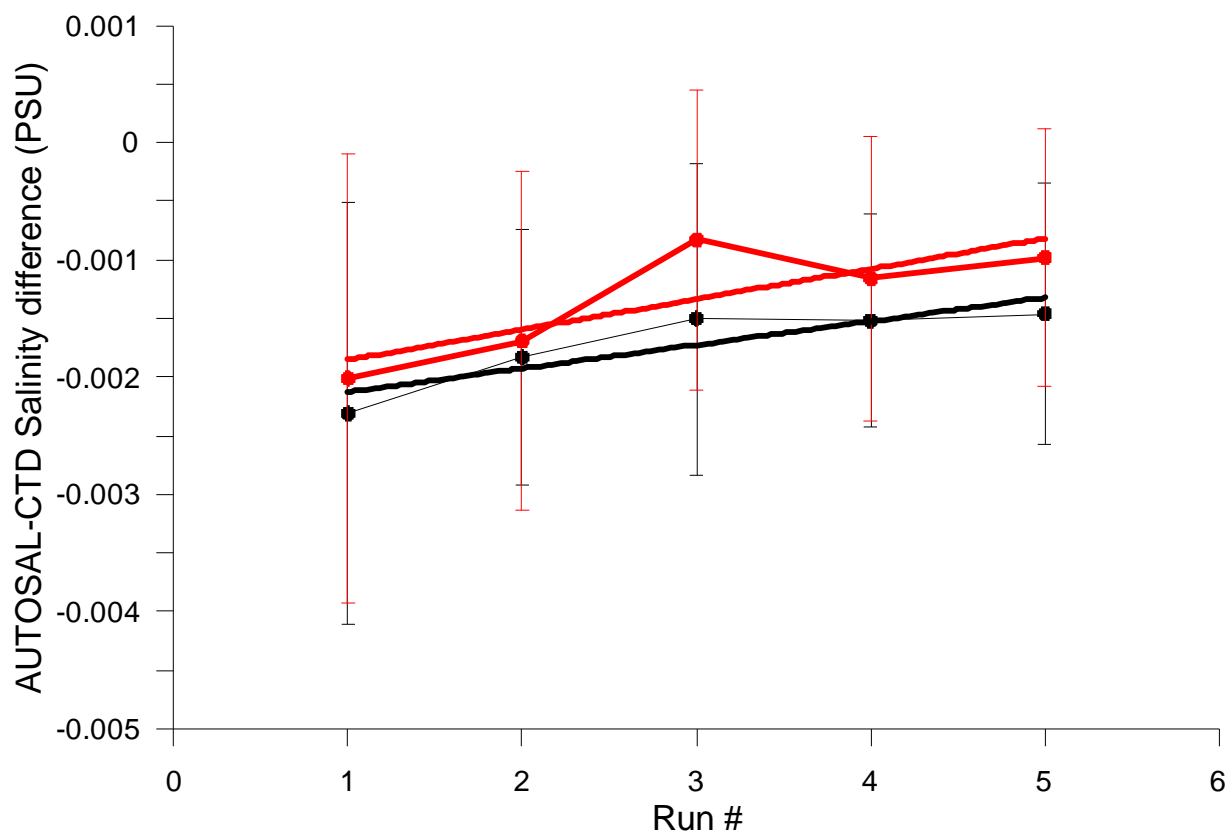


Figure 11 Autosal 8400B CTD salinity offset for the primary (in black) and secondary (in red) conductivity sensors (a) SBE 9P 0743 based on 256 salinity samples (5 runs) during 45 cruise of R/V *Akademik Ioffe*. Vertical bars show standard deviation of each run. Thick lines denote linear fits.

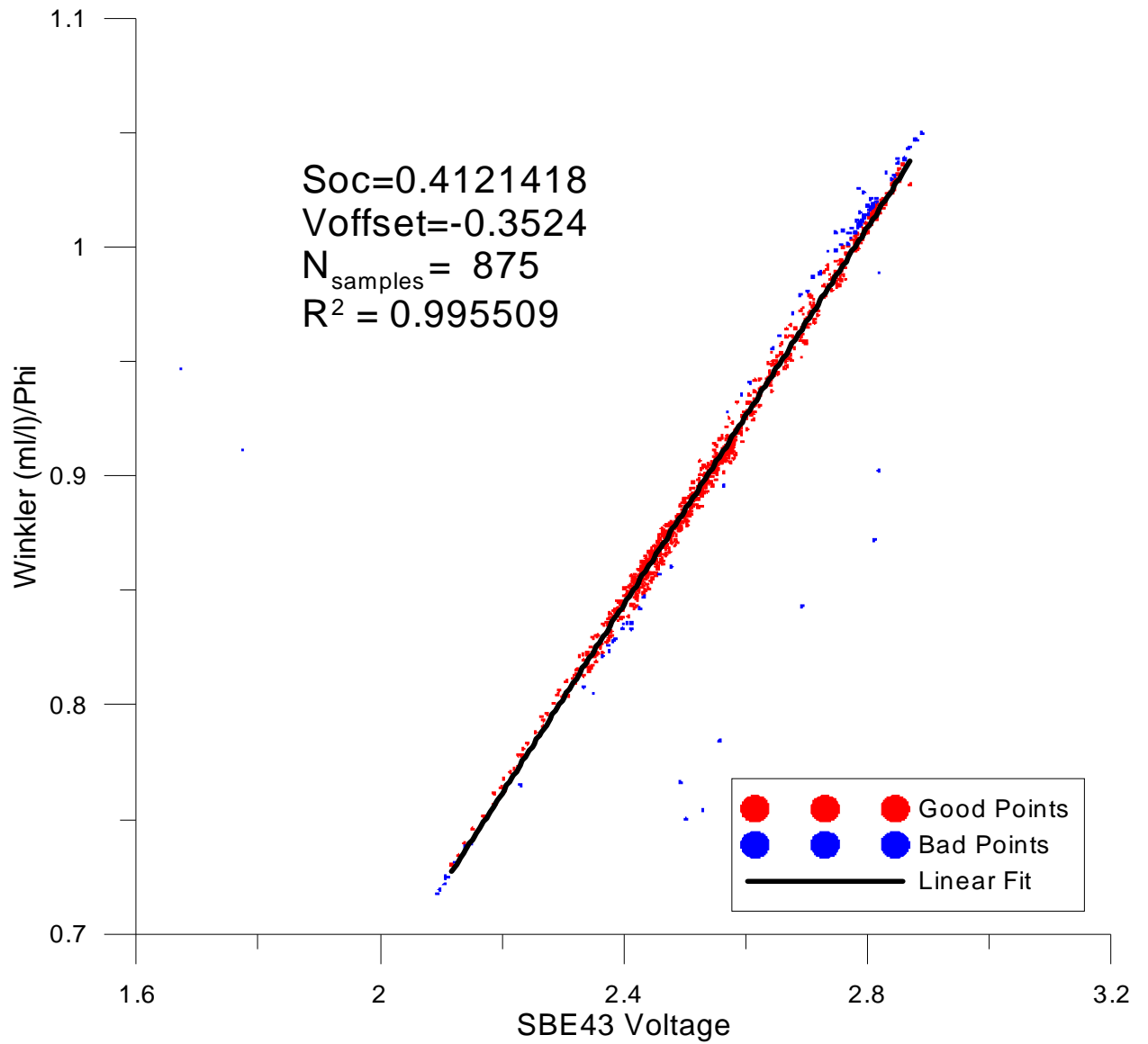


Figure 12 Regression line for Winkler oxygen divided by ϕ versus SBE 43 output voltage for the sill sections.

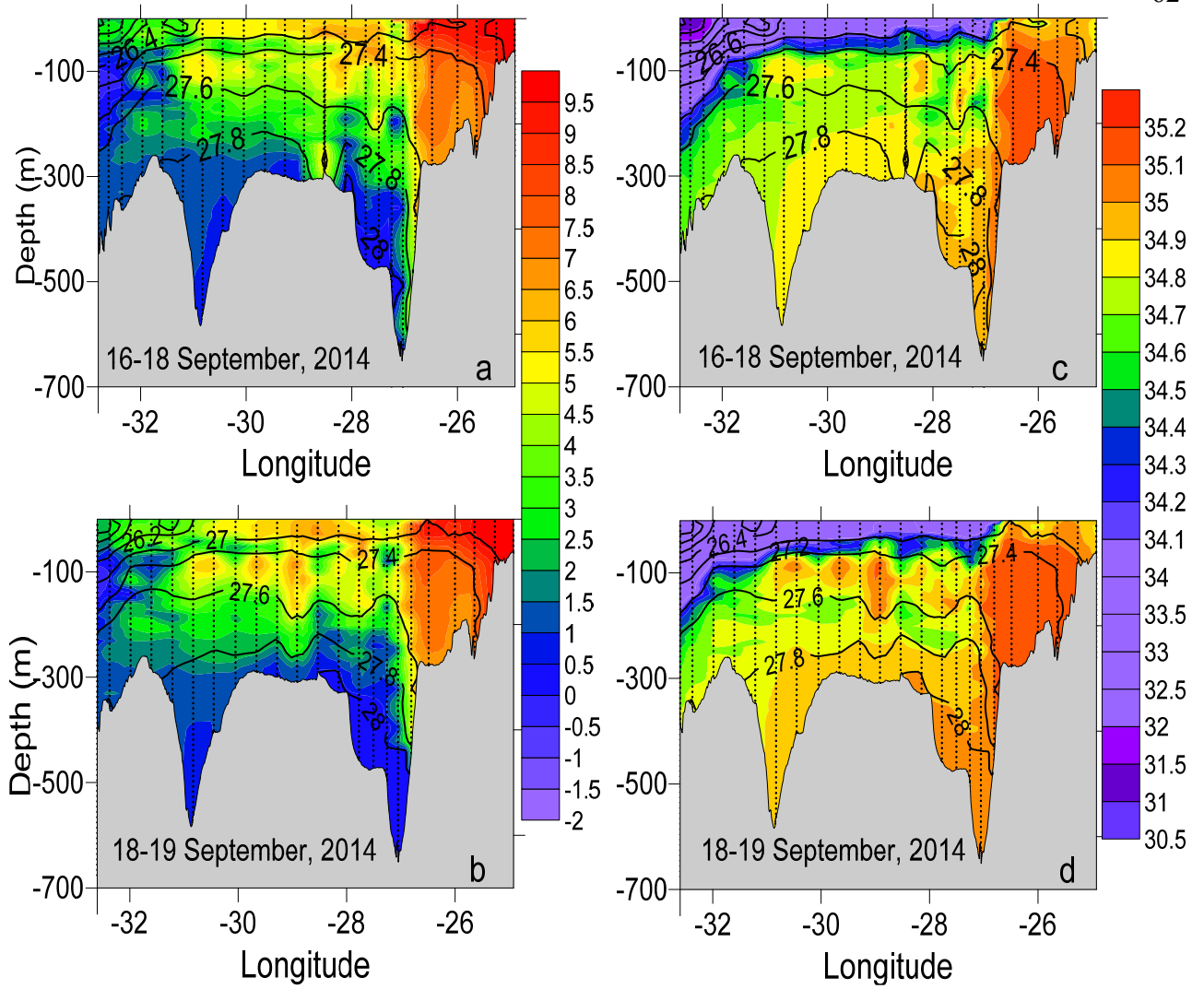


Figure 13 The vertical distribution of potential temperature (a, b) and salinity (c, d) between Greenland and Iceland 16-18 September 2014 and 18-19 September 2014. Density is shown in black.

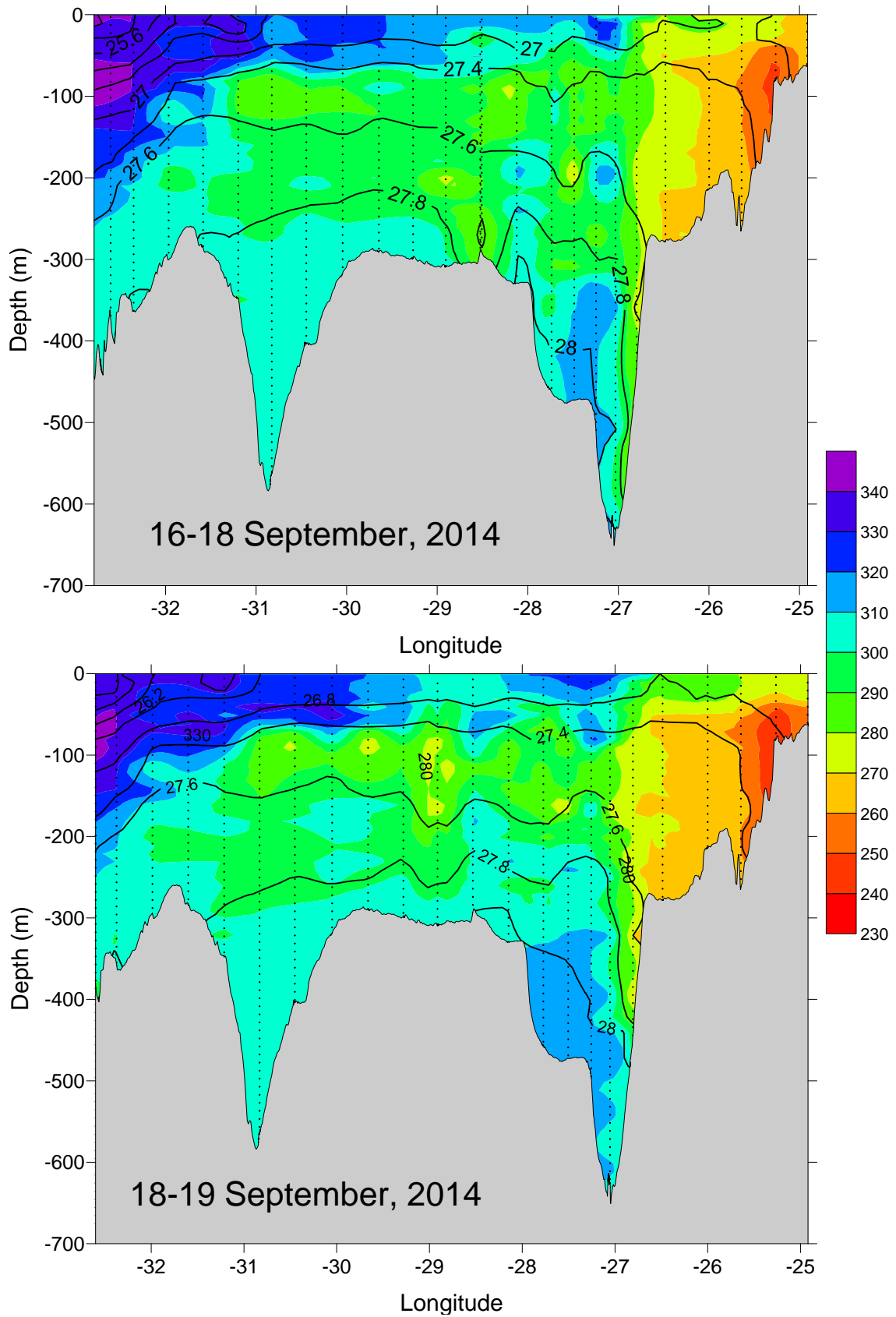


Figure 14 The vertical distribution of dissolved oxygen between Greenland and Iceland 16-18 September 2014 and 18-19 September 2014. Density is shown in black.

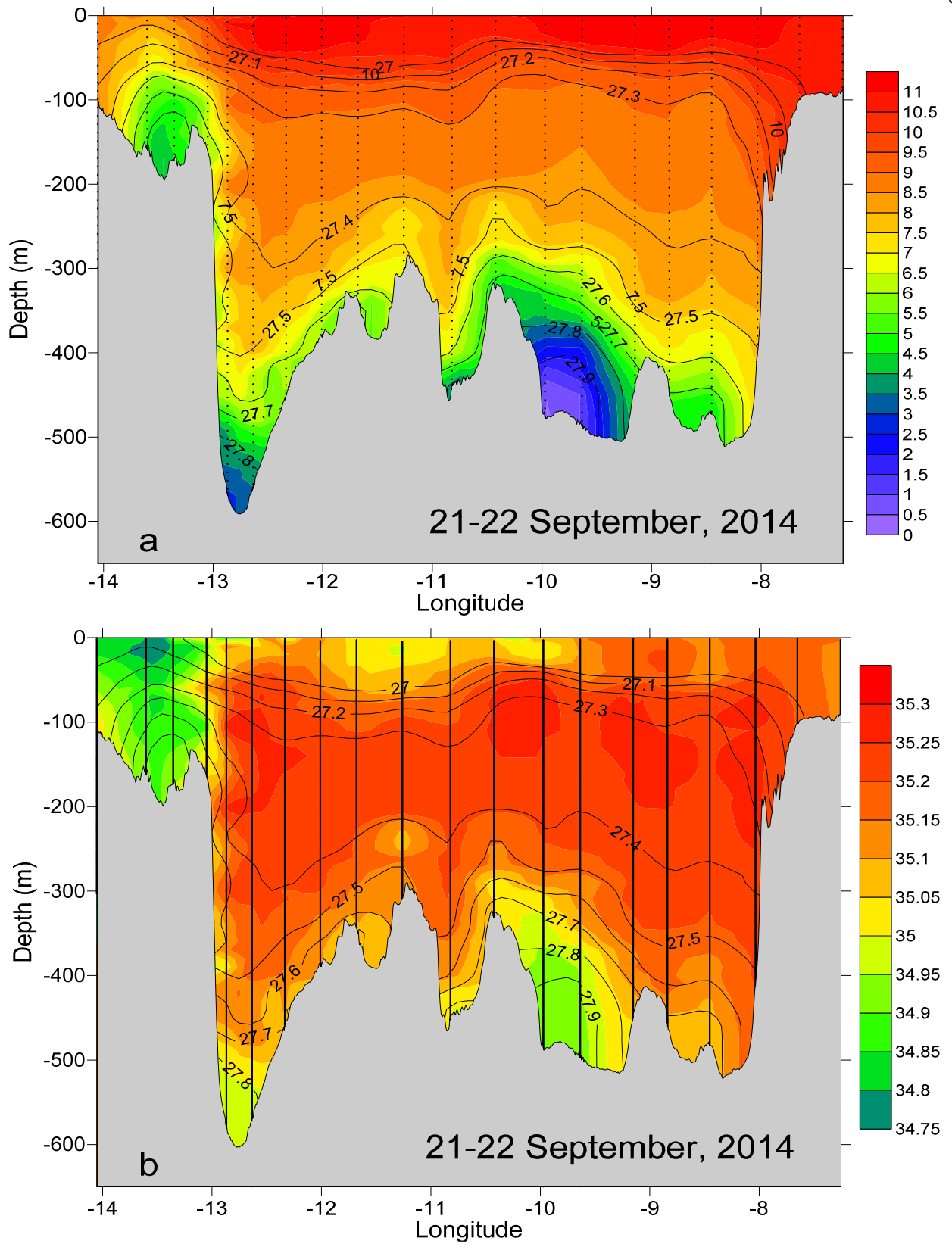


Figure 15 The vertical distribution of potential temperature (a) and salinity (b) between Iceland and Faroe Islands 21-22 September 2014. Density is shown in black.

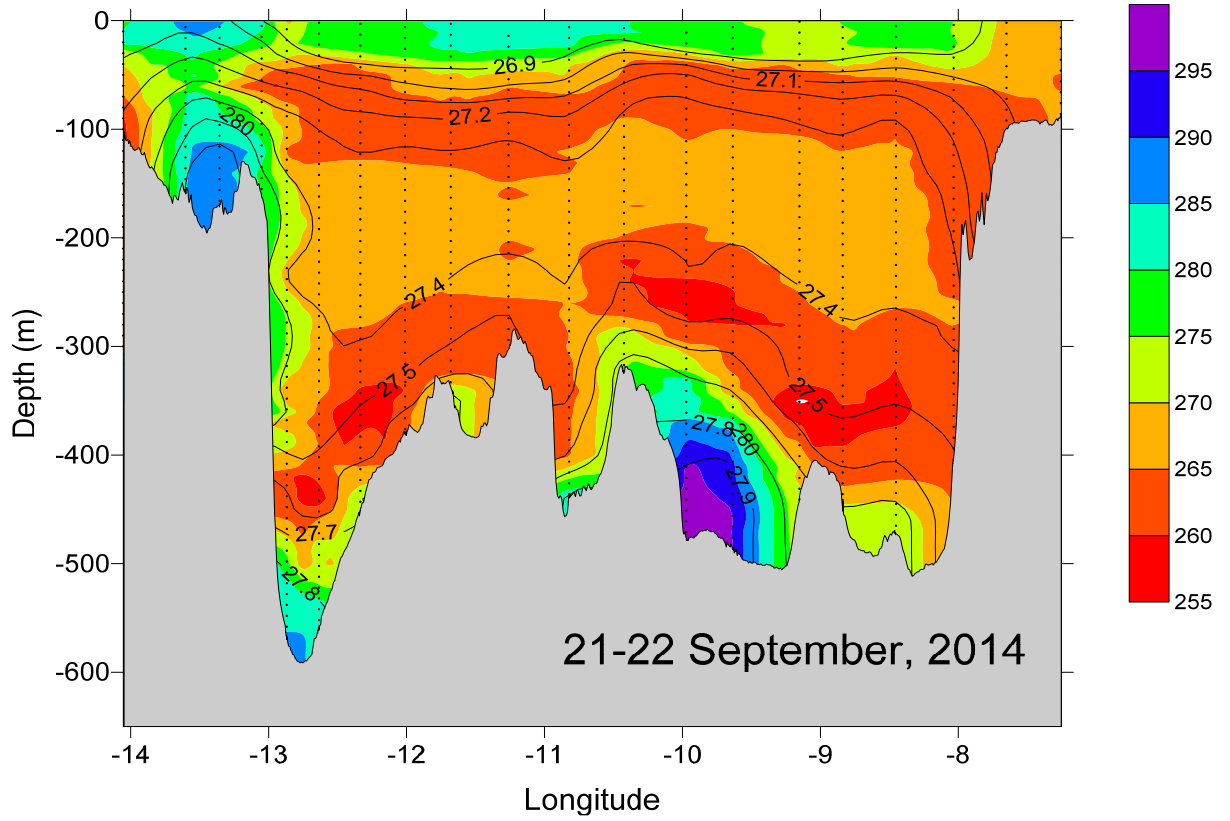


Figure 16 The vertical distribution of dissolved oxygen between Iceland and Faroe Islands 21-22 September 2014. Density is shown in black.

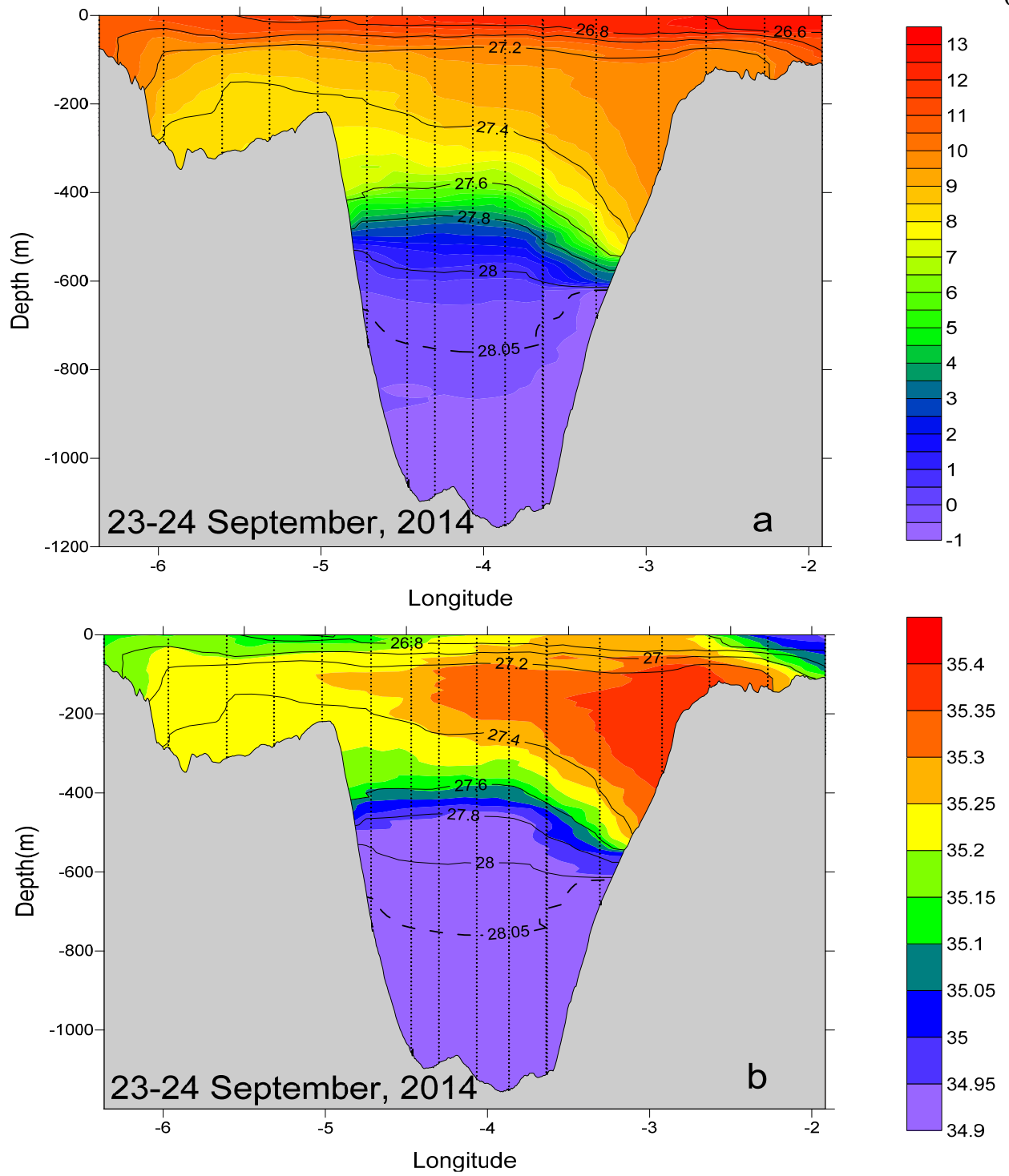


Figure 17 The vertical distribution of potential temperature (a) and salinity (b) between Shetlands and Faroe Islands 23-24 September 2014. Density is shown in black.

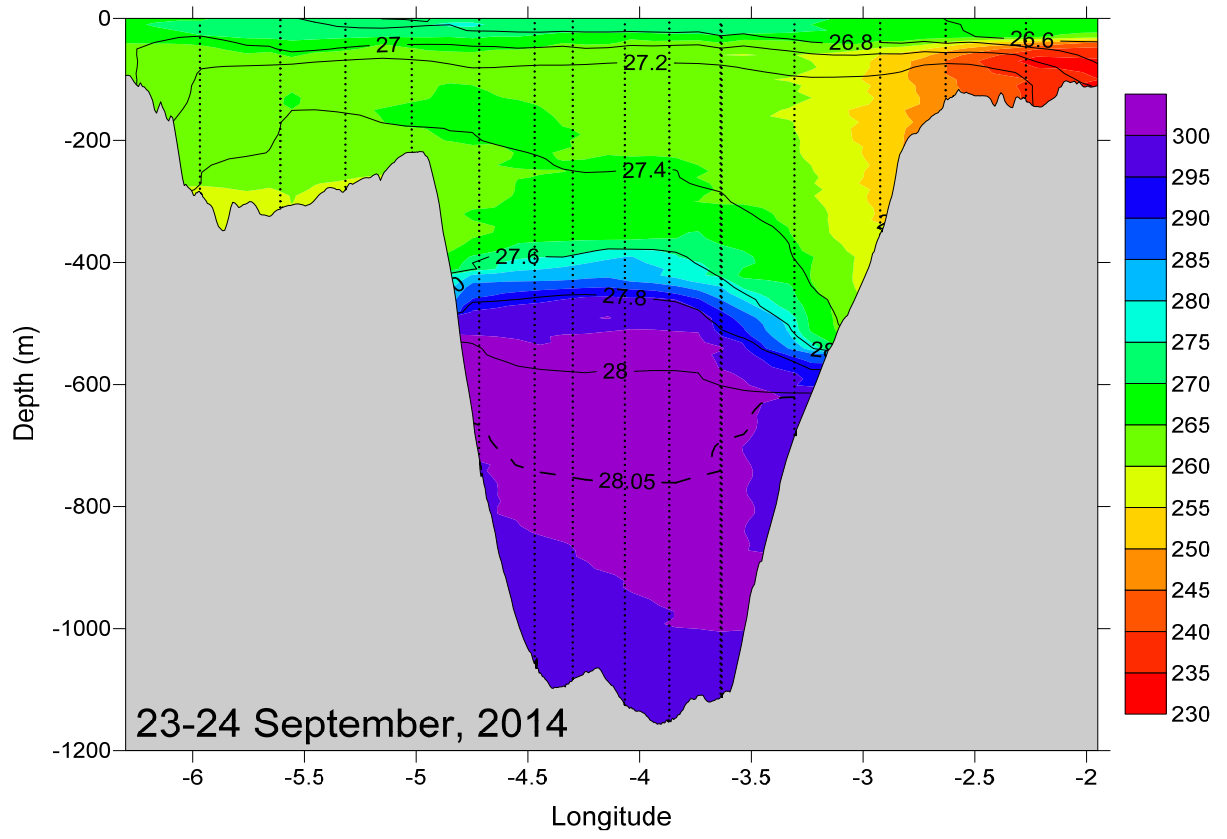


Figure 18 The vertical distribution of dissolved oxygen between Shetlands and Faroe Islands 23-24 September 2014. Density is shown in black.